

DI-Retinex: Digital-Imaging Retinex Theory for Low-Light Image Enhancement

Shangquan Sun · Wenqi Ren · Jingyang Peng · Fenglong Song · Xiaochun Cao

Received: date / Accepted: date

Abstract Many existing methods for low-light image enhancement (LLIE) based on Retinex theory ignore important factors that affect the validity of this theory in digital imaging, such as noise, quantization error, non-linearity, and dynamic range overflow. In this paper, we propose a new expression called Digital-Imaging Retinex theory (DI-Retinex) through theoretical and experimental analysis of Retinex theory in digital imaging. Our new expression includes an offset term in the enhancement model, which allows for pixel-wise brightness contrast adjustment with a non-linear mapping function. In addition, to solve the low-light enhancement problem in an unsupervised manner, we propose an image-adaptive masked reverse degradation loss in Gamma space. We also design a variance suppression loss for regulating the additional offset term. Extensive experiments show that our proposed method outperforms all existing unsupervised methods in terms of visual quality,

model size, and speed. Our algorithm can also assist downstream face detectors in low-light, as it shows the most performance gain after the low-light enhancement compared to other methods.

Keywords Low-light image enhancement · Retinex theory · face recognition

1 Introduction

In low-light conditions, digital imaging often suffers from a number of degradations, such as low visibility and high levels of noise. While professional equipment and techniques such as long exposure, fill light, and large-aperture lenses can help alleviate these issues, many amateur photographers still struggle with low-light images. Therefore, there is a need for a portable and efficient low-light image enhancement (LLIE) algorithm that can effectively restore underexposed images.

Some fundamental works, e.g., Retinex theory (Land and McCann, 1971; Land, 1977), have attempted to explain the relation among scene radiance reaching human eyes, material reflectance, and source illumination. Many LLIE algorithms and models have been designed based on this theory. However, it is important to note that the original theory was developed for radiance reaching the retina, rather than for measuring imaging intensity in computer vision. Some LLIE works have recognized the issue of amplified noise after enhancement, but there are other important factors, such as quantization error, non-linearity, and dynamic range overflow, that have not been thoroughly discussed. Simply applying Retinex theory from optics to computer vision can lead to imprecision and incompleteness in LLIE.

In this study, we conduct a theoretical analysis of the various factors that can contribute to noise, quantization error,

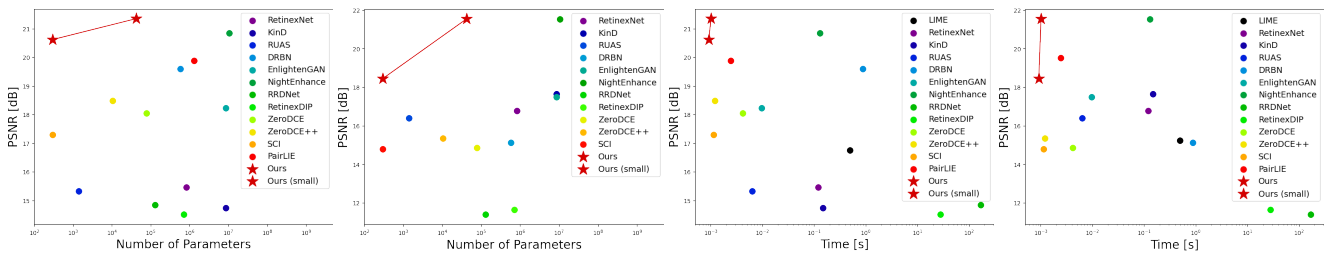
Shangquan Sun
Institute of Information Engineering, Chinese Academy of Sciences, Beijing 100085, China.
The School of Cyber Security, University of Chinese Academy of Sciences, Beijing 100049, China.
sunshangquan@iie.ac.cn

Wenqi Ren
The School of Cyber Science and Technology, Shenzhen Campus of Sun Yat-sen University, Shenzhen 518107, China.
renwq3@mail.sysu.edu.cn

Jingyang Peng
Huawei Noah's Ark Lab.
pengjingyang1@huawei.com

Fenglong Song
Huawei Noah's Ark Lab.
songfenglong@huawei.com

Xiaochun Cao
The School of Cyber Science and Technology, Shenzhen Campus of Sun Yat-sen University, Shenzhen 518107, China.
caoxiaochun@mail.sysu.edu.cn



(a) PSNR vs. model size on LOL-v1 (b) PSNR vs. model size on LOL-v2 (c) PSNR vs. run time on LOL-v1 (d) PSNR vs. run time on LOL-v2

Fig. 1: The trade-off between performance, and inference time and model size. Our method can achieve the best low-light enhancement performance with the smallest parameter number or at the fastest speed consistently.

non-linearity, and dynamic range compression when applying Retinex theory to digital imaging. We propose an extended version of Retinex theory specifically designed for computer vision called Digital-Imaging Retinex theory (DI-Retinex). Through our analysis, we demonstrate the existence of an offset with a non-zero mean and an amplified variance that can be caused by these factors when applying DI-Retinex theory to low-light image enhancement.

Building on the observation and analysis of the DI-Retinex theory, we design a brightness contrast adjustment algorithm that addresses the LLIE problem using a lightweight network consisting of three convolutional layers. The network predicts the contrast and brightness coefficients in the brightness contrast adjustment function and enhances degraded images by plugging predictions in the function. To guide the network towards generating optimal coefficient pairs, we use a masked reverse degradation loss and a variance suppression loss, which enable the network to learn in a zero-shot manner¹, without requiring paired or unpaired training data.

To sum up, our contributions can be summarized as:

- We analyze Retinex theory from the perspective of optics and computational photography and discuss the variation when transferring it to digital imaging. In addition to noise, Retinex theory should also involve quantization error, non-linearity, and dynamic range overflow in its formulation. As such, we propose a new DI-Retinex theory specifically for LLIE.
- We present a contrast brightness function to solve the LLIE problem derived from DI-Retinex theory. In addition, we propose a masked reverse degradation loss with Gamma encoding and a variance suppression loss to guide the network in a zero-shot learning manner.
- Extensive experiments demonstrate that the proposed method outperforms all the zero-shot and unsupervised learning-based LLIE methods in terms of visual quality, objective metrics, model size and speed. Moreover, our

approach can be used as a preprocessing step for downstream tasks such as detection.

2 Related Works

2.1 Classic Retinex Theory

Land and McCann (Land and McCann, 1971; Land, 1977) conducted a series of photometrical experiments, showing the scene radiance reaching human eye is the product of an intrinsic reflectance and incident illumination, which is named as Retinex Theory. It is formally written as follows,

$$\mathbf{I}^e = \mathbf{L} \odot \mathbf{R}, \quad (1)$$

where \odot denotes Hadamard product, \mathbf{I}^e means radiance reaching human eye, \mathbf{L} is illuminance, and \mathbf{R} is reflectance. For images under different exposure conditions but with an identical scene, reflectance R keeps unchanged since it is determined by and only related to the intrinsic material property of object surface. This also implies that sensation of color is mainly dependent on reflectance.

Many model-based methods employ Retinex theory for better modeling (Wang et al., 2013, 2014; Fu et al., 2014, 2016b; Guo et al., 2016; Fu et al., 2016a; Cai et al., 2017; Fu et al., 2018; Li et al., 2018b; Ren et al., 2018; Xu et al., 2020a). In recent years, deep learning with powerful learning ability and inference speed dominates the field of LLIE (Wei et al., 2018; Zhang et al., 2019b; Wang et al., 2019a,b; Fan et al., 2020; Yang et al., 2021b; Li et al., 2018a; Liu et al., 2021; Ma et al., 2022). Nearly one-third of deep learning methods also adopt Retinex theory for the sake of better enhancement effect and physical explanation (Li et al., 2021a). Therefore, a theoretical analysis of Retinex theory in digital photography is vital for establishing a valid physical model.

Note that the classic Retinex Theory has an assumption of proper exposure and the experiments of Land and McCann (Land and McCann, 1971; Land, 1977) with a telescopic photometer conclude that Eq. 1 holds for “eye” rather than camera. Simply borrowing Eq. 1 for solving LLIE

¹ Zero-shot learning in low-level vision tasks represents the method requiring neither paired or unpaired training data, in contrast to its concept in high-level visual tasks (Li et al., 2021a; Zhang et al., 2019a).

problem may be inaccurate and incomplete due to violation of the assumption and condition.

Many existing methods (Jobson et al., 1997b,a; Ma et al., 2022; Wang et al., 2019a; Liu et al., 2021; Ying et al., 2017) presumably regard the reflectance component of Retinex theory as the final enhanced result, which is not what Retinex theory originally means and affects the final performance (Li et al., 2021a). Other methods (Li et al., 2018b; Zhang et al., 2019b; Ren et al., 2018) notice the existence of amplified noise. But they neglect other involved errors, e.g., quantization error and dynamic range compression, when transferring Retinex theory from optics to digital imaging.

2.2 Model-based LLIE Methods

The earlier LLIE methods use histogram equalization (HE) (Pizer, 1990; Abdullah-Al-Wadud et al., 2007) in global level (Coltuc et al., 2006; Ibrahim and Kong, 2007) and local region (Lee et al., 2013a; Stark, 2000). Other methods utilize Retinex-theory variants including classic Retinex theory (Fu et al., 2016b; Guo et al., 2016; Wang et al., 2014; Cai et al., 2017; Fu et al., 2016a; Xu et al., 2020a), single-scale Retinex (Jobson et al., 1997b), multi-scale Retinex (Jobson et al., 1997a), adaptive multi-scale Retinex (Lee et al., 2013b), Naturalness Retinex theory (Wang et al., 2013), Robust Retinex theory (Li et al., 2018b; Ren et al., 2018), for designing physically explicable algorithms where degraded image is decomposed into reflectance and illuminance during iterative optimization. There are also some methods (Dong et al., 2010; Li et al., 2015) transforming LLIE problem into a dehazing problem. The S-curve in photography can also be used to enhance underexposed image (Yuan and Sun, 2012).

2.3 Data-Drive LLIE Methods

Supervised Learning. With the developing of deep learning, the earliest deep learning-based LLIE methods focus on learning the mapping from low-light image to normal exposed one on paired training set. Various network architectures are developed for better enhancement, including a stacked-sparse denoising autoencoder in LLNet (Lore et al., 2017), U-Net (Chen et al., 2018), a multi-branch network named MBLLN (Lv et al., 2018), Retinex-Net composed of a Decom-net and an Enhance-net (Wei et al., 2018), a lightweight LightenNet (Li et al., 2018a), a frequency decomposition network (Cai et al., 2018), a decoder network extracting global and local features (Wang et al., 2019a), siamese network (Chen et al., 2019), 3D U-Net (Jiang and Zheng, 2019; Zhang et al., 2021), progressive Retinex network (Wang et al., 2019b), three-branch

subnetworks (Zhang et al., 2019b; Yang et al., 2021b), a complex Encoder-Decoder (Ren et al., 2019), a frequency-based decomposition-and-enhancement model (Xu et al., 2020b), a model integrating semantic segmentation (Fan et al., 2020), an edge-enhanced multi-exposure fusion network (Zhu et al., 2020b), residual network (Wang et al., 2020), a Retinex-inspired unrolling model by architecture search (Liu et al., 2021, 2022), Signal-to-Noise-Ratio (SNR)-aware transformer (Xu et al., 2022), a deep color consistent network (Zhang et al., 2022), a deep unfolding Retinex network (Wu et al., 2022), a normalizing flow model (Wang et al., 2022), Gamma correction model Wang et al. (2023a), contrastive self-distillation (Fu et al., 2023a), segmentation assisting model (Wu et al., 2023), structure-aware generator (Xu et al., 2023), vision Transformers (Cai et al., 2023) and diffusion models (Wang et al., 2023b; Yi et al., 2023). The above-mentioned architectures tend to be complicated and a large scale of paired training set with low/normal exposed images are necessary for training the networks. Large model size impedes fast inference speed. Besides, collecting large paired datasets are time-consuming and expansive in terms of human labours.

Semi-Supervised Learning. Several semi-supervised learning (SSL) methods (Yang et al., 2020, 2021a) use a deep recursive band network (DRBN) to learn a linear band representation between the pair of low-light image and corresponding ground-truth. For unpaired data, a perceptual quality-driven adversarial learning is adopted for guiding enhancement. The requirement of paired data still restricts the flexibility of the SSL methods.

Unpaired-supervised Learning. To alleviate the problem of lacking paired training data, unpaired supervised learning (UL) requires a set of normal exposed images unpaired with low-light images. EnlightenGAN (Jiang et al., 2021) employs adversarial learning with a local-global discriminator structure and a perceptual loss of self-regularization. Night-Enhance (Jin et al., 2022) enhances night image with dark regions and light effects by a layer decomposition network and a light-effects suppression network with the guidance of multiple unsupervised layer-specific prior losses. However, in many common scenarios unpaired normally exposed images are still lacking or of low quality. The enhancement quality of UL methods highly relies on the quality of normally exposed images.

Zero-Shot Learning. To fully get rid of the limitation of paired data, zero-shot learning only needs low-light images for training. ExCNet (Zhang et al., 2019a) is composed of a neural network to estimate the S-curve to adjust luminance and map from back-lit input to enhanced output. The network is trained by minimizing a block-based energy expression as loss function. The idea of S-curve is adopted in Zero-DCE (Guo et al., 2020) and Zero-DCE++ (Li et al., 2021b) where a network estimating inter-

mediate light-enhancement curve is used to restore input image iteratively. They design four sophisticated loss terms to regulate spatial consistency, exposure level, color constancy, and illumination smoothness. RRDNet (Zhu et al., 2020a) solves underexposed problem by decomposing reflectance, illumination and noise components by a three-branch network with three loss terms aiming at Retinex reconstruction, texture enhancement and illumination-guided noise estimation. RetinexDIP (Zhao et al., 2021) combines Deep Image Prior and Retinex decomposition and is guided by a group of component characteristics-related losses. SCI (Ma et al., 2022) incorporates a self-calibrated illumination module for the acceleration for training, a cooperative fidelity loss term and a smoothness loss term to achieve enhancement effect intrinsically. PairLIE (Fu et al., 2023b) leverages the pair of low-light images to train a self-learning network based on Retinex theory. They are facing an unsatisfactory enhancement performance due to either delicate loss terms or the incompleteness of classic Retinex theory in LLIE task.

3 Analysis of Retinex Theory in Low-Light

In this section, we first show the existence and cause of four factors influencing the expression of the classic Retinex theory, i.e., noise, quantization error, non-linearity mapping, and dynamic range overflow. Then a novel expression of DI-Retinex theory and its corresponding enhancement model are given based on the analysis.

3.1 Imaging Noise

When scene radiance reaches imaging devices, various sources of noise consisting of read noise (Janesick, 2007; Mackay et al., 2001), dark current noise (Moon et al., 2007; Healey and Kondepudy, 1994), photon shot noise (Schottky, 1918; Blanter and Büttiker, 2000), source follower noise (Antal et al., 2001) etc., are reported and should be taken into account (Haus, 2000). Therefore, Retinex theory is rewritten by taking noise into account, i.e.,

$$\mathbf{I} = \mathbf{L} \odot \mathbf{R} + \epsilon, \quad (2)$$

where ϵ is the combination of all significant noise sources during digital imaging. Among them, photon shot and dark current noise are theoretically modeled by Poisson distribution with parameters equal to ideal incoming photon and generated electrons respectively (Blanter and Büttiker, 2000; Moon et al., 2007). Though read noise, sometimes modeled by a Gaussian distribution, can be approximated by a Poisson distribution as well (Alter et al., 2006). In this work, we denote all noise sources as a whole by ϵ .

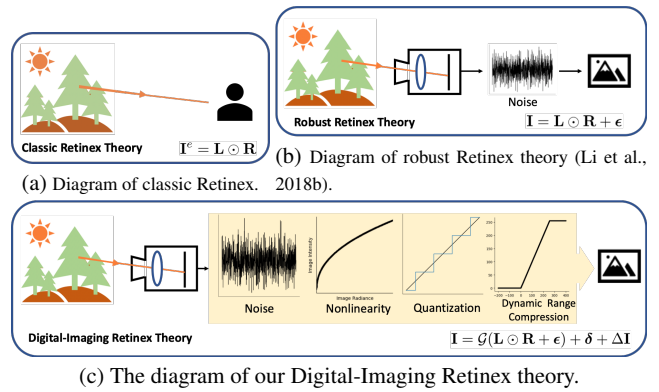


Fig. 2: The classic Retinex theory is targeted for scene radiance directly incident into human eye as shown in 2a. Some methods, e.g., (Li et al., 2018b; Zhang et al., 2019b) consider the noise as shown in 2b. However, many other factors including quantization error, non-linearity due to camera response and dynamic range overflow due to physical limitation, are ignored. Our DI-Retinex theory in 2c takes all of them into consideration.

3.2 Non-linearity.

In a digital camera, an analog-to-digital converter (ADC) is deployed to convert voltage value with a range of $[0, +\infty)$ to pixel intensity with a restricted range $[0, 255]$ in RGB color space. A non-linear response function achieves the conversion, compensates the difference of human adaptation in dark and bright regions according to Weber’s Law (Weber, 1831), and suppresses representation space. The non-linear function can be commonly modeled by a Gamma transformation or Gamma encoding as follows (Mann and Picard, 1994; Mitsunaga and Nayar, 1999):

$$\mathcal{G}(\mathbf{I}) = \mu + \lambda \mathbf{I}^\gamma, \quad (3)$$

where γ is a coefficient set to nearly 0.5 empirically, e.g., $1/2.2$, and μ, λ are two camera-specific parameters measuring bias and scale respectively.

3.3 Quantization error

Besides introducing non-linearity, the ADC converts a continuous voltage signal to a discrete N -bit value. For example, in RGB ($N = 8$) and RAW ($N = 16$) color space, there are $2^8 = 256$ and $2^{16} = 65536$ possible pixel values for each channel, respectively. However, the conversion from continuous space to discrete one yields a quantization error that can be expressed by a uniform distribution:

$$\delta_{i,j} \sim \mathcal{U}\left(-\frac{q}{2}, \frac{q}{2}\right), \quad (4)$$

where $\delta_{i,j}$ is the (i, j) -th item of a quantization error δ , $\frac{q}{2}$ is the half of least significant bit q . The discrete intensity can

be formulated by continuous intensity plus a quantization noise, i.e., $\mathbf{I}_{disc.} = \mathbf{I}_{cont.} + \delta$.

3.4 Dynamic Range Overflow

Another problem when transferring Retinex theory from human eyes to digital imaging is dynamic range limitation. Human eyes are known to have a significantly large dynamic range compared to vision sensors (Banterle et al.). Therefore, scene dynamic range is presumably within the perceptual dynamic range of human eyes in the classic Retinex theory. However, a considerable scene dynamic range may exceed the physical tolerance of imaging devices. Therefore, a clamp function \mathcal{C}_0^k is defined as Eq. 5 to clip all exceeding values.

$$\mathcal{C}_0^k(x) = \begin{cases} 0, & x < 0 \\ k, & x > k \end{cases}, \quad (5)$$

where k is the max pixel value, e.g., $k = 255$ in RGB space. By defining a masked offset matrix $\Delta\mathbf{I}$, clamp function can also be expressed as follows,

$$\mathcal{C}_0^k(\mathbf{I}) = \mathbf{I} + \Delta\mathbf{I} \quad (6)$$

where $\Delta\mathbf{I}$ has zero items at the pixels whose intensity $\mathbf{I}_{i,j} \in [0, k]$ and non-zero values $\Delta\mathbf{I}_{i,j} = k - \mathbf{I}_{i,j}$ with $\mathbf{I}_{i,j} > k$ or $\Delta\mathbf{I}_{i,j} = -\mathbf{I}_{i,j}$ with $\mathbf{I}_{i,j} < 0$.

3.5 Digital-Imaging Retinex Theory

Combining all aforementioned factors, we reformulate the classic Retinex theory as follows:

$$\mathbf{I} = \mathcal{G}(\mathbf{L} \odot \mathbf{R} + \epsilon) + \delta + \Delta\mathbf{I}, \quad (7)$$

The image irradiance perceived by the imaging device is ideal scene radiance $\mathbf{L} \odot \mathbf{R}$ plus a noise term. Then a camera response function \mathcal{G} is applied to the noisy irradiance. Finally, a quantization noise and a masked offset due to dynamic range compression are added. A comparison of the diagrams of our DI-Retinex theory and previous Retinex theories is shown in Fig. 2. Despite the complicated expression, it can be utilized to derive an efficient LLIE model.

3.6 LLIE Model based on DI-Retinex

The existing LLIE methods assuming \mathbf{R} as a final enhanced image use an enhancement function $\mathbf{I}_h = \alpha \odot \mathbf{I}_l$ with a network predicting $f(\mathbf{I}_l) = \alpha$. We extend its formulation by proving Theorem 1 involving an offset β .

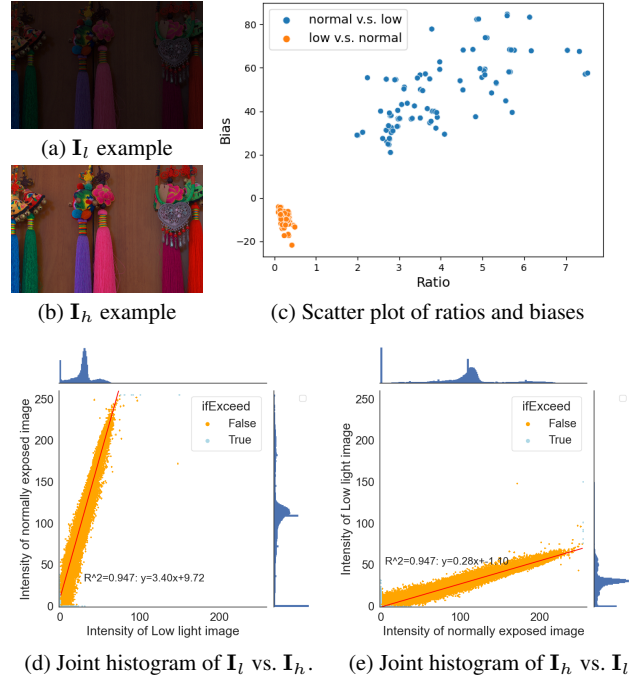


Fig. 3: The statistical experiments for showing the existence of β with a non-negligible magnitude and the existence of β' with a small magnitude.

Theorem 1 Given an underexposed image $\mathbf{I}_l \in \mathbb{R}^{H \times W}$ and one of its possible corresponding properly-exposed images $\mathbf{I}_h \in \mathbb{R}^{H \times W}$, $\exists \alpha, \beta \in \mathbb{R}^{H \times W}$ such that the following relation holds,

$$\mathbf{I}_h \approx \alpha \mathbf{I}_l + \beta. \quad (8)$$

Proof For a low-light and a normally exposed image, their expressions of DI-Retinex theory can be obtained

$$\begin{cases} \mathbf{I}_l = \mathcal{G}(\mathbf{L}_l \odot \mathbf{R} + \epsilon_l) + \delta_l + \Delta\mathbf{I}_l \\ \mathbf{I}_h = \mathcal{G}(\mathbf{L}_h \odot \mathbf{R} + \epsilon_h) + \delta_h + \Delta\mathbf{I}_h. \end{cases} \quad (9)$$

Note that \mathbf{R} keeps unchanged because reflectance components are determined by the intrinsic physical characteristics of scene objects. The expression of \mathbf{I}_h can be formulated as a function of \mathbf{I}_l as,

$$\mathbf{I}_h \approx \alpha \mathbf{I}_l + \beta, \quad (10)$$

$$\text{where } \begin{cases} \alpha = (\mathbf{L}_h \odot \mathbf{L}_l)^\gamma \\ \beta = \mu + \delta_h + \Delta\mathbf{I}_h - \alpha \odot (\mu + \delta_l + \Delta\mathbf{I}_l), \end{cases} \quad (11)$$

The notation of \odot means element-wise division between two matrices. The complete derivation of Eq. 10 is attached in the appendix. Note that with the assumption of flux consistency along time dimension across spatial pixels during receiving radiance in a short period, α can be further treated as a constant matrix.

Some may argue that the noise term β in Eq. 10 can be regarded as $\mathbf{0}$ due to the magnitude difference between the signal and the offset term β . However, we can show its mean is hardly zero, and a factor of α^2 considerably amplifies its variance. The detailed discussion is given in the appendix. We also conduct statistical experiments on a low light and normally exposed image pair from LOL-v1 (Wei et al., 2018). We plot the joint histogram of paired pixels as shown in Fig. 3. The dots in orange are those of $\mathbf{I} \in (0, k)$ and the dots in light blue are those of $\mathbf{I} = k$ or $\mathbf{I} = 0$ representing the pixels may have dynamic range overflow. A linear regression of $\mathbf{I}_h = \alpha\mathbf{I}_l + \beta$ is done for the dots $\mathbf{I}_h < k$. The regressed line is plotted in red and its coefficients are attached beside the line. The regression is fitted well by the linear model with a R^2 close to 1. From the statistical experiment, we find β has a non-negligible magnitude.

4 Method

Based on the extended DI-Retinex theory, we notice that directly regarding reflectance \mathbf{R} as the final enhanced result is inappropriate. Similarly, only estimating a single matrix α such that the enhanced image $\tilde{\mathbf{I}}_h = \alpha\mathbf{I}_l$ is also inaccurate. This is because there exists an offset β between the normal image \mathbf{I}_h and proportionally enhanced image $\alpha\mathbf{I}_l$. Therefore, we adopt a contrast brightness adjustment function involving a flexible offset for efficient enhancement.

4.1 Contrast Brightness Adjustment Function

The algorithm commonly used in brightness adjustment (Fredrik Lundh and Contributors) is as follows:

$$f(\mathbf{I}; a) = a\mathbf{I}, \quad (12)$$

where a is a brightness adjustment coefficient ranging from 0 to infinity. When $a < 1$, the image becomes dimmer, and when $a = 0$ it turns entirely black. When $a = 1$, the image keep unchanged. When $a > 1$, the image becomes brighter. The algorithm proportionally enhances pixel intensity and thus may generate images with improper contrast.

The algorithm commonly used in contrast adjustment (Fredrik Lundh and Contributors) is as follows:

$$\begin{aligned} f(\mathbf{I}; a) &= a\mathbf{I} + (1 - a)\bar{\mathbf{I}} \\ &= a(\mathbf{I} - \bar{\mathbf{I}}) + \bar{\mathbf{I}}, \end{aligned} \quad (13)$$

where a is a contrast adjustment coefficient ranging from 0 to infinity and $\bar{\mathbf{I}}$ is the average intensity of the input image. When a equals 0 or 1, the image becomes a solid gray image or keeps unchanged, respectively. The idea is to enlarge the contrast range $\mathbf{I} - \bar{\mathbf{I}}$ of zero mean and then add the average

intensity $\bar{\mathbf{I}}$ back to make sure the brightness of the image remains unchanged.

However, both Eq. 12 and Eq. 13 cannot adjust contrast and brightness simultaneously. Therefore, a contrast brightness adjustment function (android gpuiimage) is used as follows:

$$f(\mathbf{I}; a, b) = a(\mathbf{I} - (1 - b)\bar{\mathbf{I}}) + (1 + b)\bar{\mathbf{I}}, \quad (14)$$

where a and b are the factors for contrast and brightness adjustment, respectively. A $b > 0$ yields a brighter output and $b < 0$ gives a dimmer one. Compared to Eq. 13, a biased average $(1 - b)\bar{\mathbf{I}}$ is subtracted from pixel intensity and later a reverse biased one $(1 + b)\bar{\mathbf{I}}$ is added back. By Eq. 14, the image can be adjusted in terms of contrast and brightness simultaneously.

Neural networks are known to be good at predicting output with a restricted range, e.g., $[-1, 1]$, while $\mathbf{a}_{i,j} \in [0, +\infty)$ and the unknown range of b make network difficult to predict them correctly. Therefore, we first make the b restricted within $[-1, 1]$ so that the network can learn to predict them better. Through substituting $\bar{\mathbf{I}}$ by the half of max pixel value $k/2$, Eq. 14 can be rewritten

$$f(\mathbf{I}; a, b) = a \left(\mathbf{I} - \frac{k}{2}(1 - b) \right) + \frac{k}{2}(1 + b). \quad (15)$$

When $a = 1$, Eq. 15 is reduced to $f(\mathbf{I}; a, b) = \mathbf{I} + bk$, where $b = 1$ turns all pixels to max intensity, namely pure white, and $b = -1$ makes all pixels non-positive, namely pure black. $b \in [-1, 1]$ increases ($b > 0$) or reduces ($b < 0$) the brightness of image. And $a \neq 1$ enlarges ($a > 1$) or reduces ($a < 1$) the contrast of image.

The coefficient $a \in [0, +\infty)$ with range to infinity also hinders the accurate prediction of network. Therefore, a mapping function $g: [-1, 1] \rightarrow [0, +\infty)$ can be introduced. We have experimented several functions g , and empirically found the following one the best.

$$a = g(c) = \tan \left(\frac{45 + (45 - \tau)c}{180} \pi \right) \quad (16)$$

where τ is a small number to avoid $a \rightarrow \infty$ causing error in program. Based on the function Eq. 15 and mapping function Eq. 16, we propose to use an enhancement network \mathcal{H} consisting of solely three 3×3 convolutional layers with parameters θ to predict pixel-wise coefficients \mathbf{a} and \mathbf{c} for efficient contrast brightness adjustment.

$$\begin{aligned} \tilde{\mathbf{I}}_h &= \mathbf{a} \left(\mathbf{I}_l - \frac{k}{2}(1 - \mathbf{b}) \right) + \frac{k}{2}(1 + \mathbf{b}) \\ &= \mathbf{a}\mathbf{I}_l + \frac{k}{2}(\mathbf{a}\mathbf{b} - \mathbf{a} + \mathbf{b} + 1), \end{aligned} \quad (17)$$

where $[\mathbf{b}, \mathbf{c}] = \mathcal{H}(\mathbf{I}_l; \theta)$, and $\mathbf{a} = g(\mathbf{c})$. The expression is in line of the proportional relationship in Eq. 10. We design two losses for guiding the parameters \mathbf{a} and \mathbf{b} to learn the features of α and β .

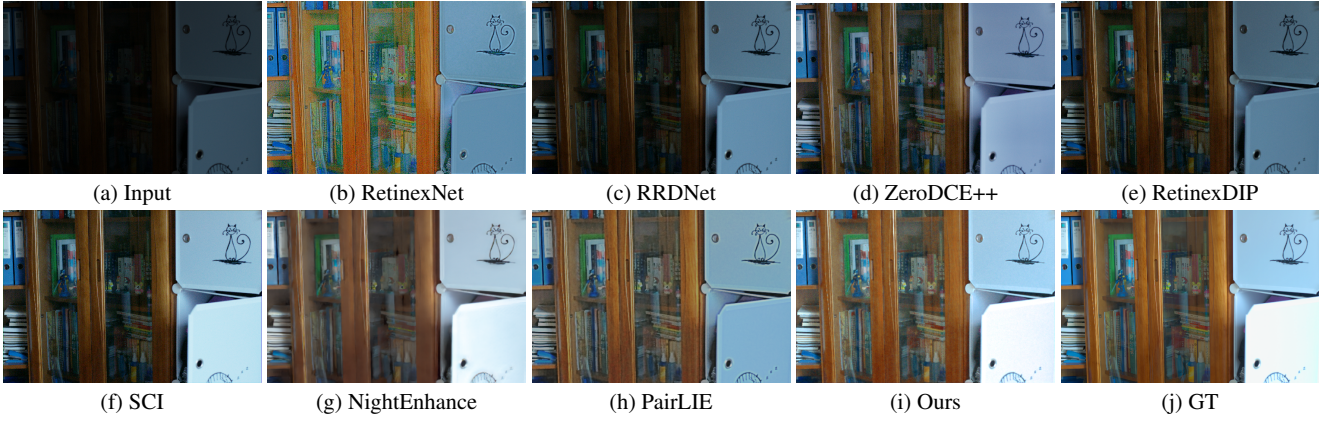


Fig. 4: A visual comparison of enhancement results on LOL-v1. Please zoom in for better visualization.

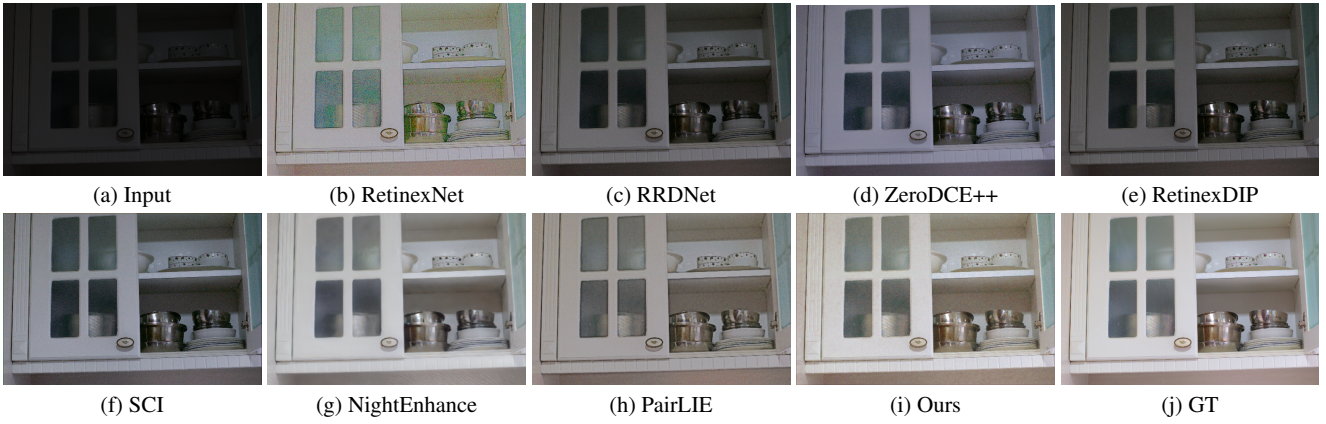


Fig. 5: A visual comparison of enhancement results on LOL-v1. Please zoom in for better visualization.

4.2 Reverse Degradation Loss

Though the enhancement based on Eq. 10 has a non-negligible offset, the reverse degradation process transforming \mathbf{I}_h to \mathbf{I}_l can be approximated to a linear proportion. We can similarly obtain

$$\mathbf{I}_l \approx \alpha' \mathbf{I}_h + \beta', \quad (18)$$

$$\text{where } \begin{cases} \alpha' = (\mathbf{L}_l \oslash \mathbf{L}_h)^\gamma \\ \beta' = \mu + \delta_l + \Delta \mathbf{I}_l - \alpha' \odot (\mu + \delta_h + \Delta \mathbf{I}_h). \end{cases} \quad (19)$$

We apply Gamma transformation to Eq. 18 and can obtain $\mathbf{I}_l^{\frac{1}{\gamma}} \approx (\mathbf{L}_l \oslash \mathbf{L}_h) \mathbf{I}_h^{\frac{1}{\gamma}}$. The detailed discussion is attached in the appendix. Therefore, we propose a masked reverse degradation loss as follows:

$$\mathcal{L}_{\mathcal{RD}} = \mathcal{M}(\tilde{\mathbf{I}}_h) \|\mathbf{I}_l^{\frac{1}{\gamma}} - \mathbf{r}' \tilde{\mathbf{I}}_h^{\frac{1}{\gamma}}\|, \quad (20)$$

where $\tilde{\mathbf{I}}_h$ is the resulting enhanced image based on Eq. 17, $\mathbf{r}' = \left(\frac{\mathbf{I}_l}{E}\right)^{1/\gamma}$ with an exposure factor $E \sim \mathcal{N}(\eta, \sigma^2)$. Based on the finding that the average exposure of a normally exposed image is nearly 0.5 (Mertens et al., 2007, 2009), η is

set to 0.5. The variance of Gaussian σ^2 specifies the divergence of targeted exposures, which will be determined in experimental settings. The power of $1/\gamma$ can suppress the magnitude of β' and its details are discussed in the appendix. We also plot the joint histogram of \mathbf{I}_h vs. \mathbf{I}_l as shown in the last plot of Fig. 3. A linear regression of $\mathbf{I}_l = \alpha \mathbf{I}_h + \beta'$ is done for the dots $\mathbf{I}_h \in (0, k)$. The regression is fitted well by the linear model with a large R^2 . As shown, β' has a small magnitude and is a negligible offset.

The mask function \mathcal{M} is defined as

$$\mathcal{M}(x) = \begin{cases} 1, & \text{if } x < k \\ 0, & \text{otherwise.} \end{cases} \quad (21)$$

The mask function is introduced because the approximate linear proportion between \mathbf{I}_l and \mathbf{I}_h is limited in regions without dynamic range compression.

4.3 Variance Suppression loss

We want the second term in Eq. 17 consisting of \mathbf{a} and \mathbf{b} to learn the feature of β in Eq. 10. We have shown that though β has a non-zero mean that yields a necessary offset

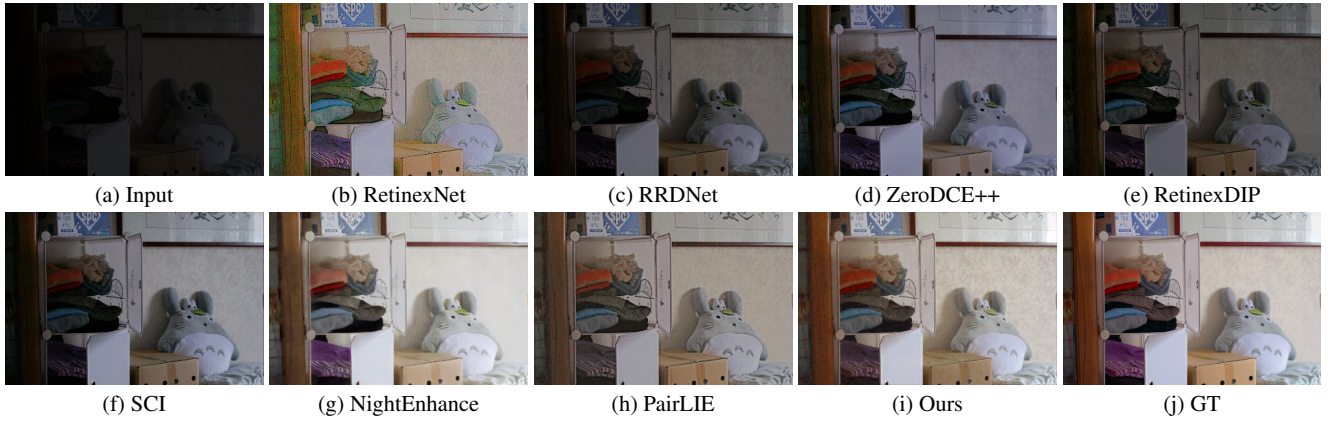


Fig. 6: A visual comparison of enhancement results on LOL-v1. Please zoom in for better visualization.

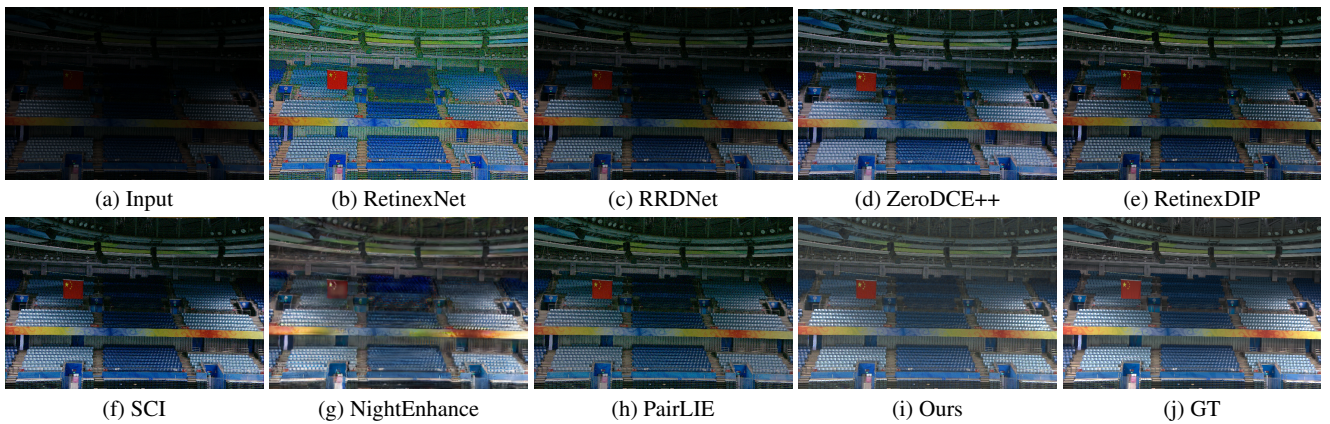


Fig. 7: A visual comparison of enhancement results on LOL-v2. Please zoom in for better visualization.

for modeling enhanced images, it has an amplified variance due to $\alpha > 1$, which will contribute to an enhanced variance of recovered images. Therefore, we design a variance suppression loss such that its variance approaches zero. The expression of the variance suppression loss is given by

$$\mathcal{L}_{VS} = \|\text{Var}(\mathbf{ab} - \mathbf{a} + \mathbf{b} + 1)\|, \quad (22)$$

where Var is computed along each channels. As a result, the overall loss of our model is as follows:

$$\mathcal{L}_{\text{overall}} = \mathcal{L}_{RD} + \mathcal{L}_{VS}. \quad (23)$$

4.4 Relation between DI-Retinex and the enhancement model

The traditional Retinex theory, originally borrowed from optics, has served as a fundamental guiding principle for numerous prior low-light enhancement works. However, it has come to our attention that the digital imaging process introduces deviations from the optical Retinex theory, resulting in the emergence of what we term the DI-Retinex theory. In accordance with this novel theory, we derive Eq. 10, wherein β

emerges as a significant term. In contrast, if we were to rely solely on the conventional Retinex theory, β would assume a value of zero. This, in turn, renders the subsequently derived enhancement model in Eq. 17, which incorporates an offset term, invalid. In summary, the proposed DI-Retinex theory ensures the presence of a non-negligible offset term in the relationship between low-light and normal images. This, in turn, substantiates the formulation of the presented enhancement model, which features an offset term. Furthermore, the DI-Retinex theory establishes a reverse relationship between low-light and normal images, enabling us to derive the reverse degradation loss.

5 Experiments

5.1 Experimental Settings

Datasets. We adopt the datasets for comparison including LOL-v1 (Wei et al., 2018), LOL-v2 (Yang et al., 2021b), and DARKFACE (Yuan et al., 2019). The details and statistics of the datasets are illustrated in the supplemental material. The number of training and test sets of LOL-v1 (Wei

et al., 2018), LOL-v2-Real (Yang et al., 2021b) and DARKFACE (Yuan et al., 2019) are illustrated in Table. 1. We randomly sample 1000 images for DARKFACE following (Li et al., 2021a; Ma et al., 2022). Note that LOL-v2 has a synthetic part and a real captured part. Since we are modeling realistic low light degradation by extended Retinex theory, we only experiment on its real part.

Table 1: The statistics of datasets.

	Train	Test
LOL-v1	485	15
LOL-v2-Real	689	100
	# of Images	# of Faces
DARKFACE	1000	37040

Baselines. We compare our methods with model-based method including LIME (Guo et al., 2016), supervised learning methods including RetinexNet (Wei et al., 2018), KinD (Zhang et al., 2019b), and RUAS (Liu et al., 2021), semi-supervised learning methods including DRBN (Yang et al., 2021a), unpaired supervised learning methods including EnlightenGAN (Jiang et al., 2021) and NightEnhance (Jin et al., 2022), and zero-shot learning methods including RRDNet (Zhu et al., 2020a), Zero-DCE (Guo et al., 2020), Zero-DCE++ (Li et al., 2021b), RetinexDIP (Zhao et al., 2021), SCI (Ma et al., 2022) and PairLIE (Fu et al., 2023b). Since our method belongs to zero-shot learning, we focus on the comparison with the existing zero-shot learning methods.

Table 2: The quantitative results of LLIE methods on LOL-v1 (Wei et al., 2018) in terms of MSE [$\times 10^3$], PSNR in dB, SSIM (Wang et al., 2004) and LPIPS (Zhang et al., 2018). The best, second best and third best results are in **red**, **blue** and **green** respectively.

	MSE↓	PSNR↑	SSIM↑	LPIPS↓
Input	12.622	7.771	0.181	0.560
LIME (Guo et al., 2016)	2.269	16.760	0.560	0.350
RetinexNet (Wei et al., 2018)	1.656	16.774	0.462	0.474
KinD (Zhang et al., 2019b)	1.431	17.648	0.779	0.175
RUAS (Liu et al., 2021)	3.920	16.398	0.537	0.350
DRBN (Yang et al., 2021a)	2.359	15.125	0.472	0.316
EnlightenGAN (Jiang et al., 2021)	1.998	17.478	0.677	0.322
RRDNet (Zhu et al., 2020a)	6.313	11.384	0.470	0.361
RetinexDIP (Zhao et al., 2021)	6.050	11.646	0.501	0.317
ZeroDCE (Guo et al., 2020)	3.282	14.857	0.589	0.335
ZeroDCE++ (Li et al., 2021b)	3.035	15.342	0.603	0.316
SCI (Li et al., 2021b)	3.496	14.780	0.553	0.332
NightEnhance (Jin et al., 2022)	1.070	21.521	0.763	0.235
PairLIE (Fu et al., 2023b)	1.419	18.463	0.749	0.290
Ours	0.784	21.542	0.766	0.219
Ours (small)	1.706	18.448	0.641	0.312

Evaluation Criteria. We employ four full-reference metrics, i.e., MSE, PSNR, SSIM (Wang et al., 2004) and LPIPS (Zhang et al., 2018), and two metrics indicating efficiency, i.e., model size and inference time. For the dataset DARKFACE (Yuan et al., 2019), a Precision-Recall curve is plotted for performance indication.

Implementations. We train our model on the training set of each dataset. We use ADAM as the optimizer with an initial learning rate of 0.001 and weight decay of 0.0001. The variance of Gaussian distribution in the reverse degradation loss is set to 0.001 and τ in Eq. 16 is set to 0.2. The network is trained for 1000 epochs. Since the network is small and learns mapping coefficients \mathbf{a} and \mathbf{b} globally, we do not crop patches during training. Batch size is set to 1. All experiments are conducted on an NVIDIA GeForce GTX 1080 GPU and implemented by PyTorch (Paszke et al., 2019). Our codes will be released.

5.2 Results on LOL-v1

We first evaluate our method on LOL-v1 (Wei et al., 2018) by comparing its LLIE performance with other existing methods. The quantitative results are shown in Table. 2. We can see that our model has the best performance in terms of MSE and PSNR. Furthermore, our method has the second-best value of SSIM and LPIPS. We also train another small version of our model by reducing internal (64 to 4) and output channels (6 to 2). The performance of our small model can still outperform most existing methods. Note that the number of parameters in our model is only 1/31 of PairLIE (Fu et al., 2023b), 1/251 of NightEnhance (Jin et al., 2022) and 1/202 of KinD (Zhang et al., 2019b).

We then give several examples for the visual comparison among the existing methods and ours in Fig. 4 to Fig. 6. We can see in Fig. 4 that only our model restores the contents in the bookshelf. In addition, in the pure white region in the bottom right corner, other methods are “afraid” of enhancing the white pixels, which are meant to be overexposed in photography, towards overexposure. However, our proposed mask function \mathcal{M} in \mathcal{L}_{RD} deals with the dynamic range overflow and enables the successful enhancement of the white pixels. In Fig. 5, most methods cannot recover the brightness of the imaging scene properly except NightEnhance (Jin et al., 2022) and ours. Compared with NightEnhance (Jin et al., 2022), our method better enhances the shadow inside the cupboard. In Fig. 6, still only ours and NightEnhance (Jin et al., 2022) can achieve the closest results to the ground-truth. However, our method restores the color of the wall with more vivid fidelity.

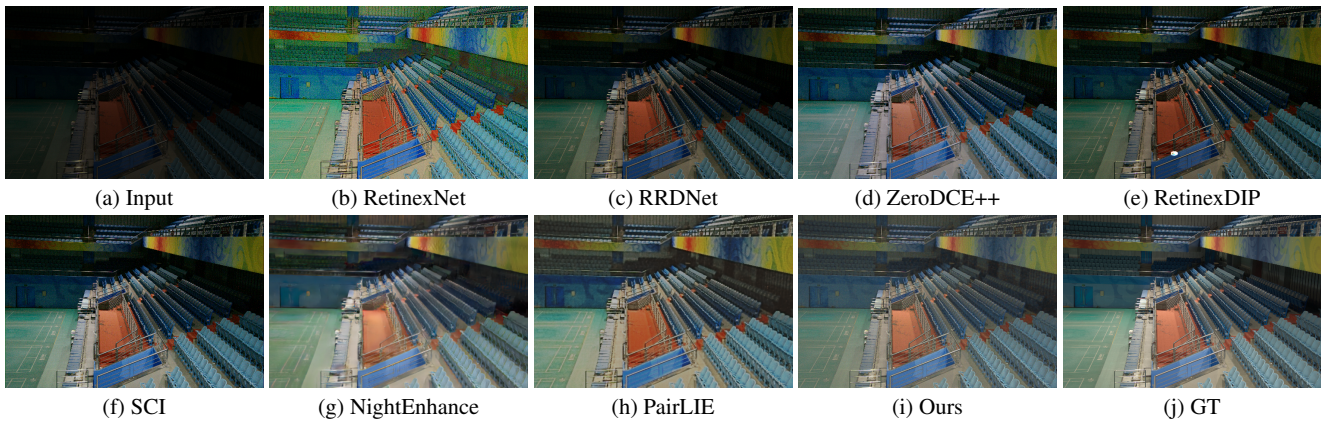


Fig. 8: A visual comparison of enhancement results on LOL-v2. Please zoom in for better visualization.

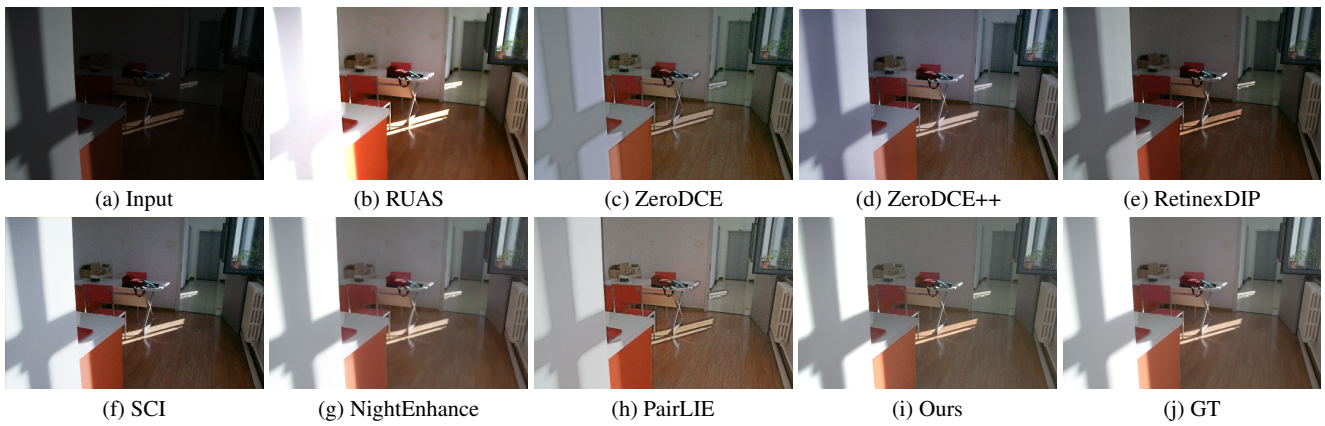


Fig. 9: A visual comparison of enhancement results on LOL-v2. Please zoom in for better visualization.

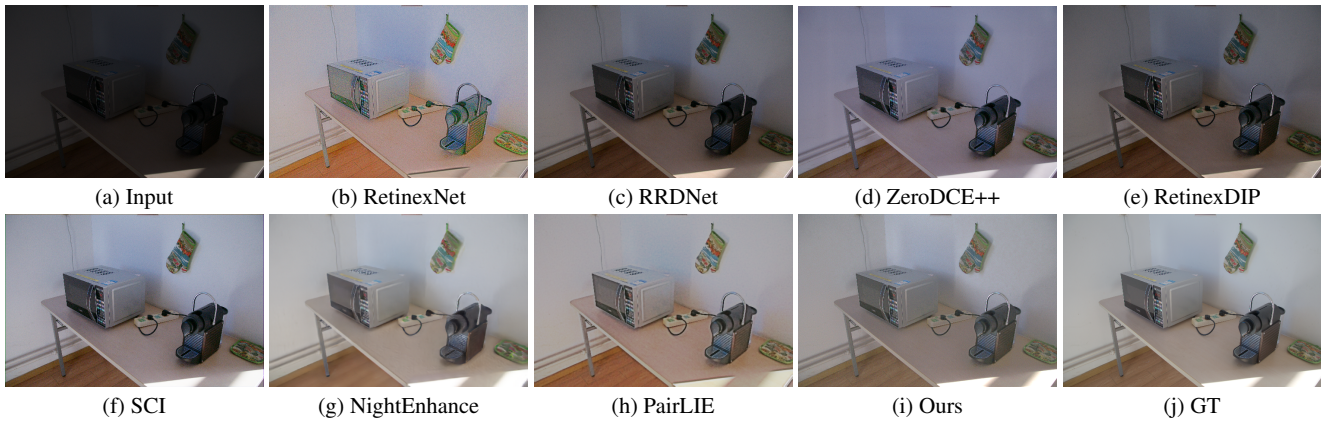


Fig. 10: A visual comparison of enhancement results on LOL-v2. Please zoom in for better visualization.

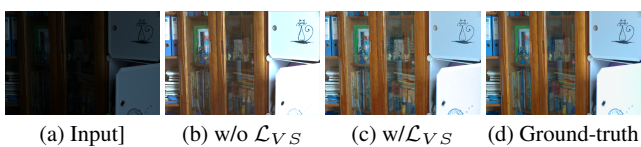


Fig. 11: The visual ablation comparison regarding \mathcal{L}_{VS} .

5.3 Results on LOL-v2

Similar to LOL-v1 (Wei et al., 2018), we evaluate our method on LOL-v2 (Yang et al., 2021b). The quantitative results are shown in Table. 3. We can see that our model has the best performance in terms of PSNR, SSIM, and LPIPS. The performance of our model with smaller size is the third best in terms of all the metrics.



Fig. 12: A visual comparison of enhancement and face detection results on DARKFACE. Please zoom in for better view.

Table 3: The quantitative results of LLIE methods on LOL-v2 (Yang et al., 2021b) in terms of MSE [$\times 10^3$], PSNR in dB, SSIM (Wang et al., 2004) and LPIPS (Zhang et al., 2018). The best, second best and third best results are in **red**, **blue** and **green** respectively.

	MSE \downarrow	PSNR \uparrow	SSIM \uparrow	LPIPS \downarrow
Input	7.634	9.718	0.190	0.333
LIME (Guo et al., 2016)	1.484	15.240	0.470	0.360
RetinexNet (Wei et al., 2018)	1.719	15.470	0.560	0.421
KinD (Zhang et al., 2019b)	4.029	14.740	0.641	0.302
RUAS (Liu et al., 2021)	2.540	15.330	0.520	0.322
DRBN (Yang et al., 2021a)	1.843	19.600	0.764	0.246
EnlightenGAN (Jiang et al., 2021)	1.209	18.230	0.610	0.309
RRDNet (Zhu et al., 2020a)	3.594	14.850	0.560	0.265
RetinexDIP (Zhao et al., 2021)	3.157	14.513	0.546	0.274
ZeroDCE (Guo et al., 2020)	1.777	18.059	0.605	0.298
ZeroDCE++ (Li et al., 2021b)	1.569	18.491	0.617	0.290
SCI (Ma et al., 2022)	2.132	17.304	0.565	0.286
NightEnhance (Jin et al., 2022)	0.819	20.850	0.724	0.329
PairLIE (Fu et al., 2023b)	0.916	19.885	0.778	0.282
Ours	0.827	21.362	0.795	0.225
Ours (small)	1.064	20.631	0.739	0.252

We also provide several illustrative examples for visually comparing our method and others in Fig. 7 to Fig. 10 sampled from LOL-v2 (Yang et al., 2021b). The non-uniform brightness in the grandstand of stadium is challenging for all LLIE methods. Among them, ours and NightEnhance (Jin et al., 2022) can generate the closest results to the ground-truth. However, NightEnhance (Jin et al., 2022) makes the red flag fade, while ours restore the color better. In Fig 9, only our solution yields the correct brightness of the white wall. In Fig. 8 and Fig. 10, our method gives the closest results to the ground-truth.

5.4 Ablation Study

We evaluate the effect of the proposed offset β , the variance suppression loss \mathcal{L}_{VS} , the reverse degradation loss \mathcal{L}_{RD} , and the mask function \mathcal{M} in \mathcal{L}_{RD} . We also conduct abla-

tion studies on the choice of scalar or matrix of predicted parameters. We also trial other formulations of the mapping function g besides Eq. 16. The expressions are listed below in Eq. 24.

$$\begin{aligned}
 g_1(c) &= \frac{1+c}{1-c+e} \\
 g_2(c) &= 3 \tanh^{-1} \left(\frac{1}{2} + \frac{1}{2}c \right) = \frac{3}{2} \log \left(\frac{3+c}{1-c+e} \right) \\
 g_3(c) &= 3 \log(g(c) + 1),
 \end{aligned} \tag{24}$$

where $e = 10^{-8}$ is a small value preventing error in program. The explanation for choosing the formulations are discussed in the appendix.

The results are shown in Table. 4. We can conclude that each of β , \mathcal{L}_{VS} , \mathcal{L}_{RD} , and \mathcal{M} leads to better enhancement. The constant parameters cannot fully encode the complex expressions of the coefficients. We show an example in Fig. 11 and the heatmap of decomposed parameters in Fig. 19 in the Appendix. For different choices of the mapping function, g_3 has the comparable performance to g . However, the double non-linearity of log and tan in g_3 yields slower speed and thus we choose g in Eq. 16.

Table 4: The results of our model with various settings on LOL-v1. The frames per second (FPS) are used for speed comparison.

	w/o β	w/o \mathcal{L}_{VS}	w/o \mathcal{L}_{RD}	w/o \mathcal{M}
PSNR	10.44	20.15	17.62	21.52
SSIM	0.476	0.721	0.656	0.757
	g_1	g_2	g_3	Ours
PSNR	17.43	20.34	21.62	21.54
SSIM	0.679	0.724	0.768	0.766
FPS	986	891	831	954
	b&c	b&c	b&c	b&c
PSNR	14.29	17.78	19.40	21.54
SSIM	0.547	0.653	0.692	0.766

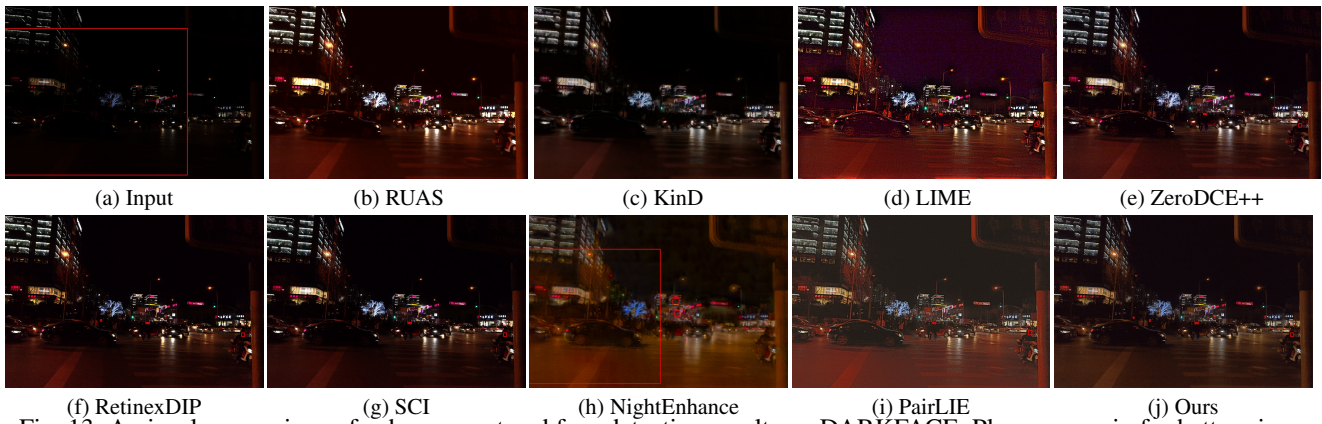


Fig. 13: A visual comparison of enhancement and face detection results on DARKFACE. Please zoom in for better view.

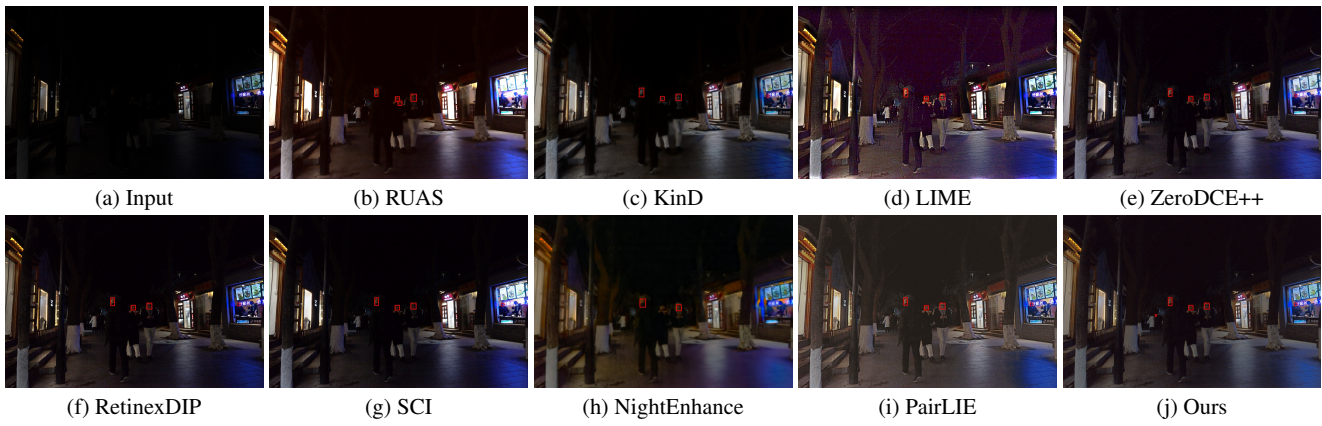


Fig. 14: A visual comparison of enhancement and face detection results on DARKFACE. Please zoom in for better view.



Fig. 15: A visual comparison of enhancement and face detection results on DARKFACE. Please zoom in for better view.

5.5 Extentions

Results on DARKFACE. Image enhancement can serve as a preprocessing for high-level downstream tasks. We thus evaluate our method on a face detection dataset in low-light conditions, i.e., DARKFACE (Yuan et al., 2019). The detector of Dual Shot Face Detector (DSFD) (Li et al., 2019) pretrained on WIDERFACE (Yang et al., 2016) is used for predicting face location. For the enhanced data through each

LLIE method, a Precision-Recall curve (PR curve) can be drawn. The stacked PR curves for all methods are shown in Fig. 16. We can see our method has the best performance. Four samples for visual comparison is illustrated in Fig. 12 to Fig. 15, where only the enhancement by our method detects the most faces correctly. Note that though some methods like NightEnhance (Jin et al., 2022) could generate brighter scenes, the introduction of more artifacts

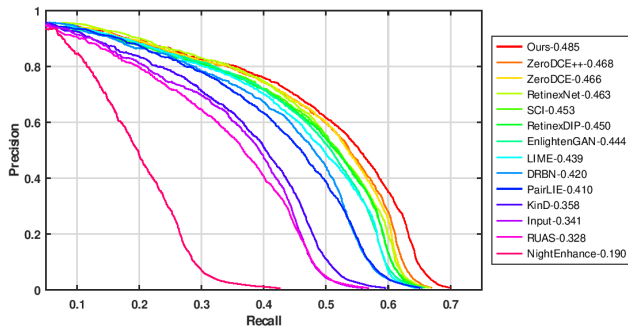


Fig. 16: The Precision-Recall Curve of performing detection on DARKFACE (Yuan et al., 2019) by DSFD (Li et al., 2019) for the LLIE methods.

and noise reduces the face detection accuracy, which is not consistently in line with human intuition.

Efficiency. As shown in Fig. 1, our methods achieve the best overall balance between visual quality and model size/run time consistently on LOL-v1 (Wei et al., 2018) and LOL-v2 (Yang et al., 2021b). Compared to NightEnhance (Jin et al., 2022), our models are much faster and small. Compared to SCI (Ma et al., 2022) and ZeroDCE++ (Li et al., 2021b), ours have much higher PSNR.

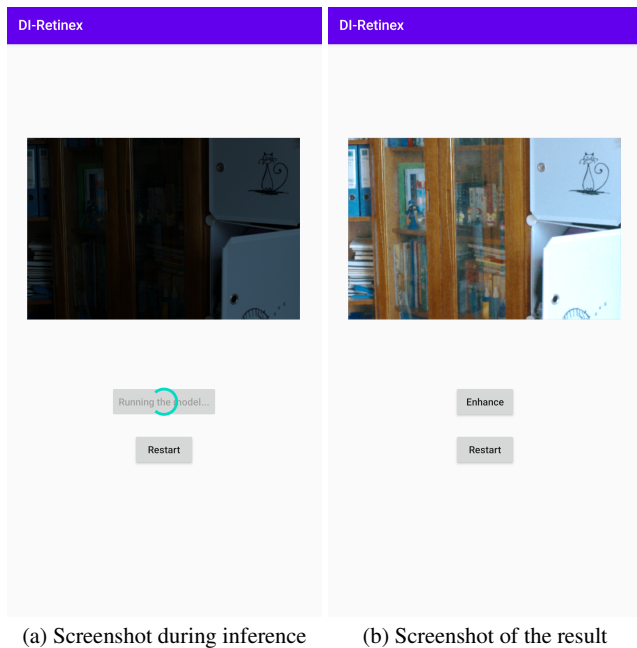


Fig. 17: The mobile implementation based on Android.

Mobile Implementation. We implement our method and create an application on Android system by Android Studio based on the repository of PyTorch on Android². As

² <https://github.com/pytorch/android-demo-app/>

seen in Fig. 17, our model can achieve an accurate enhancement result on a type of mobile device, Huawei Mate 20. The runtime on the device is 0.439 second per frame. The experiment shows the feasibility of applying our lightweight model to mobile application. We also trial implementing several other lightweight methods on the mobile device and test their inference time. For NightEnhance (Jin et al., 2022) and PairLIE (Fu et al., 2023b), the buffer usage exceeds the device limit during converting datatype. The results are shown in Table 5. Note that the mobile implementation of PyTorch is on CPU.

Table 5: The average runtime [s] and PSNR of the lightweight LLIE models on the mobile device, Huawei Mate 20.

	ZeroDCE	ZeroDCE++	SCI	Ours
runtime	0.822	0.701	0.762	0.439
PSNR	14.86	15.34	14.78	21.54

6 Conclusion

In this work, we extend the classic Retinex theory, targeted initially at formulating scene radiance reaching human eyes, to a complex form taking noise, quantization error, non-linearity response function, and dynamic range limitation into consideration. By incorporating these factors, we demonstrate that the LLIE problem can be modeled through a pixel-wise linear restoration function that includes an offset with non-zero mean, which was previously ignored in other works. Besides we introduce a contrast brightness adjustment function for enhancing low-light images in a zero-shot learning manner. A masked reverse degradation loss in Gamma space and a variance suppression loss for regulating the offset feature are derived from the proposed LLIE model. The reverse degradation process darkens an enhanced image back to the input low-light image, thereby reducing the offset. Our method can achieve the best performance with the fewest parameters and the least runtime.

References

- M. Abdullah-Al-Wadud, M. H. Kabir, M. A. A. Dewan, and O. Chae. A dynamic histogram equalization for image contrast enhancement. *IEEE Transactions on Consumer Electronics*, 53(2):593–600, 2007.
- F. Alter, Y. Matsushita, and X. Tang. An intensity similarity measure in low-light conditions. In *European Conference on Computer Vision*, pages 267–280. Springer, 2006.
- android gpuimage. Source code for `gpuimagecontrastfilter`. [EB/OL]. <https://github.com/cats-oss/android-gpuimage/blob/master/library/src/main/java/jp/co/cyberagent/android/gpuimage/filter/>.

- T. Antal, M. Droz, G. Györgyi, and Z. Rácz. 1/f noise and extreme value statistics. *Physical review letters*, 87(24):240601, 2001.
- F. Banterle, A. Artusi, K. Debattista, and A. Chalmers. Advanced high dynamic range imaging: Theory and practice,(2011).
- Y. M. Blanter and M. Büttiker. Shot noise in mesoscopic conductors. *Physics reports*, 336(1-2):1–166, 2000.
- B. Cai, X. Xu, K. Guo, K. Jia, B. Hu, and D. Tao. A joint intrinsic-extrinsic prior model for retinex. In *Proceedings of the IEEE international conference on computer vision*, pages 4000–4009, 2017.
- J. Cai, S. Gu, and L. Zhang. Learning a deep single image contrast enhancer from multi-exposure images. *IEEE Transactions on Image Processing*, 27(4):2049–2062, 2018.
- Y. Cai, H. Bian, J. Lin, H. Wang, R. Timofte, and Y. Zhang. Retinexformer: One-stage retinex-based transformer for low-light image enhancement. In *Proceedings of the IEEE/CVF International Conference on Computer Vision (ICCV)*, pages 12504–12513, October 2023.
- C. Chen, Q. Chen, J. Xu, and V. Koltun. Learning to see in the dark. In *Proceedings of the IEEE conference on computer vision and pattern recognition*, pages 3291–3300, 2018.
- C. Chen, Q. Chen, M. N. Do, and V. Koltun. Seeing motion in the dark. In *Proceedings of the IEEE/CVF International Conference on Computer Vision*, pages 3185–3194, 2019.
- D. Coltuc, P. Bolon, and J.-M. Chassery. Exact histogram specification. *IEEE Transactions on Image processing*, 15(5):1143–1152, 2006.
- X. Dong, Y. Pang, and J. Wen. Fast efficient algorithm for enhancement of low lighting video. In *ACM SIGGRAPH 2010 Posters*, pages 1–1, 2010.
- M. Fan, W. Wang, W. Yang, and J. Liu. Integrating semantic segmentation and retinex model for low-light image enhancement. In *Proceedings of the 28th ACM international conference on multimedia*, pages 2317–2325, 2020.
- A. C. Fredrik Lundh and Contributors. Source code for pil.imageenhance. [EB/OL]. https://pillow.readthedocs.io/en/stable/_modules/PIL/ImageEnhance.html#Contrast.
- H. Fu, W. Zheng, X. Meng, X. Wang, C. Wang, and H. Ma. You do not need additional priors or regularizers in retinex-based low-light image enhancement. In *Proceedings of the IEEE/CVF Conference on Computer Vision and Pattern Recognition (CVPR)*, pages 18125–18134, June 2023a.
- Q. Fu, C. Jung, and K. Xu. Retinex-based perceptual contrast enhancement in images using luminance adaptation. *IEEE Access*, 6:61277–61286, 2018.
- X. Fu, Y. Sun, M. LiWang, Y. Huang, X.-P. Zhang, and X. Ding. A novel retinex based approach for image enhancement with illumination adjustment. In *2014 IEEE International Conference on Acoustics, Speech and Signal Processing (ICASSP)*, pages 1190–1194. IEEE, 2014.
- X. Fu, D. Zeng, Y. Huang, Y. Liao, X. Ding, and J. Paisley. A fusion-based enhancing method for weakly illuminated images. *Signal Processing*, 129:82–96, 2016a.
- X. Fu, D. Zeng, Y. Huang, X.-P. Zhang, and X. Ding. A weighted variational model for simultaneous reflectance and illumination estimation. In *Proceedings of the IEEE conference on computer vision and pattern recognition*, pages 2782–2790, 2016b.
- Z. Fu, Y. Yang, X. Tu, Y. Huang, X. Ding, and K.-K. Ma. Learning a simple low-light image enhancer from paired low-light instances. In *Proceedings of the IEEE/CVF Conference on Computer Vision and Pattern Recognition*, pages 22252–22261, 2023b.
- C. Guo, C. Li, J. Guo, C. C. Loy, J. Hou, S. Kwong, and R. Cong. Zero-reference deep curve estimation for low-light image enhancement. In *Proceedings of the IEEE/CVF Conference on Computer Vision and Pattern Recognition*, pages 1780–1789, 2020.
- X. Guo, Y. Li, and H. Ling. Lime: Low-light image enhancement via illumination map estimation. *IEEE Transactions on image processing*, 26(2):982–993, 2016.
- H. A. Haus. *Electromagnetic noise and quantum optical measurements*. Springer Science & Business Media, 2000.
- G. E. Healey and R. Kondepudy. Radiometric ccd camera calibration and noise estimation. *IEEE Transactions on Pattern Analysis and Machine Intelligence*, 16(3):267–276, 1994.
- H. Ibrahim and N. S. P. Kong. Brightness preserving dynamic histogram equalization for image contrast enhancement. *IEEE Transactions on Consumer Electronics*, 53(4):1752–1758, 2007.
- J. R. Janesick. Photon transfer. SPIE, 2007.
- H. Jiang and Y. Zheng. Learning to see moving objects in the dark. In *2019 IEEE/CVF International Conference on Computer Vision (ICCV)*, pages 7323–7332, 2019. doi: 10.1109/ICCV.2019.00742.
- Y. Jiang, X. Gong, D. Liu, Y. Cheng, C. Fang, X. Shen, J. Yang, P. Zhou, and Z. Wang. Enlightengan: Deep light enhancement without paired supervision. *IEEE Transactions on Image Processing*, 30:2340–2349, 2021.
- Y. Jin, W. Yang, and R. T. Tan. Unsupervised night image enhancement: When layer decomposition meets light-effects suppression. In *European Conference on Computer Vision*, pages 404–421. Springer, 2022.
- D. J. Jobson, Z.-u. Rahman, and G. A. Woodell. A multiscale retinex for bridging the gap between color images and the human observation of scenes. *IEEE Transactions on Image processing*, 6(7):965–976, 1997a.
- D. J. Jobson, Z.-u. Rahman, and G. A. Woodell. Properties and performance of a center/surround retinex. *IEEE transactions on image processing*, 6(3):451–462, 1997b.
- E. H. Land. The retinex theory of color vision. *Scientific american*, 237(6):108–129, 1977.
- E. H. Land and J. J. McCann. Lightness and retinex theory. *Josa*, 61(1):1–11, 1971.
- C. Lee, C. Lee, and C.-S. Kim. Contrast enhancement based on layered difference representation of 2d histograms. *IEEE transactions on image processing*, 22(12):5372–5384, 2013a.
- C.-H. Lee, J.-L. Shih, C.-C. Lien, and C.-C. Han. Adaptive multi-scale retinex for image contrast enhancement. In *2013 International Conference on Signal-Image Technology & Internet-Based Systems*, pages 43–50. IEEE, 2013b.
- C. Li, J. Guo, F. Porikli, and Y. Pang. Lightnet: A convolutional neural network for weakly illuminated image enhancement. *Pattern recognition letters*, 104:15–22, 2018a.
- C. Li, C. Guo, L.-H. Han, J. Jiang, M.-M. Cheng, J. Gu, and C. C. Loy. Low-light image and video enhancement using deep learning: A survey. *IEEE Transactions on Pattern Analysis & Machine Intelligence*, (01):1–1, 2021a.
- C. Li, C. G. Guo, and C. C. Loy. Learning to enhance low-light image via zero-reference deep curve estimation. In *IEEE Transactions on Pattern Analysis and Machine Intelligence*, 2021b. doi: 10.1109/TPAMI.2021.3063604.
- J. Li, Y. Wang, C. Wang, Y. Tai, J. Qian, J. Yang, C. Wang, J. Li, and F. Huang. Dsfed: Dual shot face detector. In *Proceedings of the IEEE Conference on Computer Vision and Pattern Recognition*, 2019.
- L. Li, R. Wang, W. Wang, and W. Gao. A low-light image enhancement method for both denoising and contrast enlarging. In *2015 IEEE international conference on image processing (ICIP)*, pages 3730–3734. IEEE, 2015.
- M. Li, J. Liu, W. Yang, X. Sun, and Z. Guo. Structure-revealing low-light image enhancement via robust retinex model. *IEEE Transactions on Image Processing*, 27(6):2828–2841, 2018b.
- R. Liu, L. Ma, J. Zhang, X. Fan, and Z. Luo. Retinex-inspired unrolling with cooperative prior architecture search for low-light image enhancement. In *Proceedings of the IEEE/CVF Conference on Computer Vision and Pattern Recognition*, pages 10561–10570, 2021.
- R. Liu, L. Ma, T. Ma, X. Fan, and Z. Luo. Learning with nested scene modeling and cooperative architecture search for low-light vision.

- IEEE Transactions on Pattern Analysis and Machine Intelligence*, 45(5):5953–5969, 2022.
- K. G. Lore, A. Akinatayo, and S. Sarkar. Llnet: A deep autoencoder approach to natural low-light image enhancement. *Pattern Recognition*, 61:650–662, 2017.
- F. Lv, F. Lu, J. Wu, and C. Lim. Mblen: Low-light image/video enhancement using cnns. In *BMVC*, volume 220, page 4, 2018.
- L. Ma, T. Ma, R. Liu, X. Fan, and Z. Luo. Toward fast, flexible, and robust low-light image enhancement. In *Proceedings of the IEEE/CVF Conference on Computer Vision and Pattern Recognition*, pages 5637–5646, 2022.
- C. D. Mackay, R. N. Tubbs, R. Bell, D. J. Burt, P. Jerram, and I. Moody. Subelectron read noise at mhz pixel rates. In *Sensors and Camera Systems for Scientific, Industrial, and Digital Photography Applications II*, volume 4306, pages 289–298. SPIE, 2001.
- S. Mann and R. Picard. Beingundigital with digital cameras. *MIT Media Lab Perceptual*, 1:2, 1994.
- T. Mertens, J. Kautz, and F. Van Reeth. Exposure fusion. In *15th Pacific Conference on Computer Graphics and Applications (PG'07)*, pages 382–390. IEEE, 2007.
- T. Mertens, J. Kautz, and F. Van Reeth. Exposure fusion: A simple and practical alternative to high dynamic range photography. In *Computer graphics forum*, volume 28, pages 161–171. Wiley Online Library, 2009.
- T. Mitsunaga and S. K. Nayar. Radiometric self calibration. In *Proceedings. 1999 IEEE computer society conference on computer vision and pattern recognition (Cat. No PR00149)*, volume 1, pages 374–380. IEEE, 1999.
- C.-R. Moon, J. Jung, D.-W. Kwon, J. Yoo, D.-H. Lee, and K. Kim. Application of plasma-doping (plad) technique to reduce dark current of cmos image sensors. *IEEE electron device letters*, 28(2):114–116, 2007.
- V. Padmavathy and R. Priya. Image contrast enhancement techniques—a survey. *International Journal of Engineering & Technology*, 7(2.33):466–469, 2018.
- S. Park, K. Kim, S. Yu, and J. Paik. Contrast enhancement for low-light image enhancement: A survey. *IEIE Transactions on Smart Processing and Computing*, 7:36–48, 2018.
- A. Paszke, S. Gross, F. Massa, A. Lerer, J. Bradbury, G. Chanan, T. Killeen, Z. Lin, N. Gimelshein, L. Antiga, et al. Pytorch: An imperative style, high-performance deep learning library. *Advances in neural information processing systems*, 32, 2019.
- S. M. Pizer. Contrast-limited adaptive histogram equalization: Speed and effectiveness stephen m. pizer, r. eugene johnston, james p. ericksen, bonnie c. yankaskas, keith e. muller medical image display research group. In *Proceedings of the first conference on visualization in biomedical computing, Atlanta, Georgia*, volume 337, page 1, 1990.
- W. Ren, S. Liu, L. Ma, Q. Xu, X. Xu, X. Cao, J. Du, and M.-H. Yang. Low-light image enhancement via a deep hybrid network. *IEEE Transactions on Image Processing*, 28(9):4364–4375, 2019.
- X. Ren, M. Li, W.-H. Cheng, and J. Liu. Joint enhancement and denoising method via sequential decomposition. In *2018 IEEE international symposium on circuits and systems (ISCAS)*, pages 1–5. IEEE, 2018.
- W. Schottky. Über spontane stromschwankungen in verschiedenen elektrizitätsleitern. *Annalen der physik*, 362(23):541–567, 1918.
- J. A. Stark. Adaptive image contrast enhancement using generalizations of histogram equalization. *IEEE Transactions on image processing*, 9(5):889–896, 2000.
- D. Vijayalakshmi, M. K. Nath, and O. P. Acharya. A comprehensive survey on image contrast enhancement techniques in spatial domain. *Sensing and Imaging*, 21(1):1–40, 2020.
- L. Wang, L. Xiao, H. Liu, and Z. Wei. Variational bayesian method for retinex. *IEEE Transactions on Image Processing*, 23(8):3381–3396, 2014.
- L.-W. Wang, Z.-S. Liu, W.-C. Siu, and D. P. Lun. Lightning network for low-light image enhancement. *IEEE Transactions on Image Processing*, 29:7984–7996, 2020.
- R. Wang, Q. Zhang, C.-W. Fu, X. Shen, W.-S. Zheng, and J. Jia. Underexposed photo enhancement using deep illumination estimation. In *Proceedings of the IEEE/CVF Conference on Computer Vision and Pattern Recognition*, pages 6849–6857, 2019a.
- S. Wang, J. Zheng, H.-M. Hu, and B. Li. Naturalness preserved enhancement algorithm for non-uniform illumination images. *IEEE transactions on image processing*, 22(9):3538–3548, 2013.
- Y. Wang, Y. Cao, Z.-J. Zha, J. Zhang, Z. Xiong, W. Zhang, and F. Wu. Progressive retinex: Mutually reinforced illumination-noise perception network for low-light image enhancement. In *Proceedings of the 27th ACM international conference on multimedia*, pages 2015–2023, 2019b.
- Y. Wang, R. Wan, W. Yang, H. Li, L.-P. Chau, and A. Kot. Low-light image enhancement with normalizing flow. In *Proceedings of the AAAI Conference on Artificial Intelligence*, volume 36, pages 2604–2612, 2022.
- Y. Wang, Z. Liu, J. Liu, S. Xu, and S. Liu. Low-light image enhancement with illumination-aware gamma correction and complete image modelling network. In *Proceedings of the IEEE/CVF International Conference on Computer Vision (ICCV)*, pages 13128–13137, October 2023a.
- Y. Wang, Y. Yu, W. Yang, L. Guo, L.-P. Chau, A. C. Kot, and B. Wen. Exposediffusion: Learning to expose for low-light image enhancement. In *Proceedings of the IEEE/CVF International Conference on Computer Vision (ICCV)*, pages 12438–12448, October 2023b.
- Z. Wang, A. C. Bovik, H. R. Sheikh, and E. P. Simoncelli. Image quality assessment: from error visibility to structural similarity. *IEEE transactions on image processing*, 13(4):600–612, 2004.
- E. H. Weber. *De Pulsu, resorptione, auditu et tactu: Annotationes anatomicae et physiologicae...* CF Koehler, 1831.
- C. Wei, W. Wang, W. Yang, and J. Liu. Deep retinex decomposition for low-light enhancement. In *British Machine Vision Conference*, 2018.
- W. Wu, J. Weng, P. Zhang, X. Wang, W. Yang, and J. Jiang. Uretinex-net: Retinex-based deep unfolding network for low-light image enhancement. In *Proceedings of the IEEE/CVF Conference on Computer Vision and Pattern Recognition*, pages 5901–5910, 2022.
- Y. Wu, C. Pan, G. Wang, Y. Yang, J. Wei, C. Li, and H. T. Shen. Learning semantic-aware knowledge guidance for low-light image enhancement. In *Proceedings of the IEEE/CVF Conference on Computer Vision and Pattern Recognition (CVPR)*, pages 1662–1671, June 2023.
- J. Xu, Y. Hou, D. Ren, L. Liu, F. Zhu, M. Yu, H. Wang, and L. Shao. Star: A structure and texture aware retinex model. *IEEE Transactions on Image Processing*, 29:5022–5037, 2020a.
- K. Xu, X. Yang, B. Yin, and R. W. Lau. Learning to restore low-light images via decomposition-and-enhancement. In *Proceedings of the IEEE/CVF Conference on Computer Vision and Pattern Recognition*, pages 2281–2290, 2020b.
- X. Xu, R. Wang, C.-W. Fu, and J. Jia. Snr-aware low-light image enhancement. In *Proceedings of the IEEE/CVF Conference on Computer Vision and Pattern Recognition*, pages 17714–17724, 2022.
- X. Xu, R. Wang, and J. Lu. Low-light image enhancement via structure modeling and guidance. In *Proceedings of the IEEE/CVF Conference on Computer Vision and Pattern Recognition (CVPR)*, pages 9893–9903, June 2023.
- S. Yang, P. Luo, C.-C. Loy, and X. Tang. Wider face: A face detection benchmark. In *Proceedings of the IEEE conference on computer vision and pattern recognition*, pages 5525–5533, 2016.
- W. Yang, S. Wang, Y. Fang, Y. Wang, and J. Liu. From fidelity to perceptual quality: A semi-supervised approach for low-light image enhancement. In *Proceedings of the IEEE/CVF conference on*

- computer vision and pattern recognition*, pages 3063–3072, 2020.
- W. Yang, S. Wang, Y. Fang, Y. Wang, and J. Liu. Band representation-based semi-supervised low-light image enhancement: Bridging the gap between signal fidelity and perceptual quality. *IEEE Transactions on Image Processing*, 30:3461–3473, 2021a.
- W. Yang, W. Wang, H. Huang, S. Wang, and J. Liu. Sparse gradient regularized deep retinex network for robust low-light image enhancement. *IEEE Transactions on Image Processing*, 30:2072–2086, 2021b.
- X. Yi, H. Xu, H. Zhang, L. Tang, and J. Ma. Diff-retinex: Rethinking low-light image enhancement with a generative diffusion model. In *Proceedings of the IEEE/CVF International Conference on Computer Vision (ICCV)*, pages 12302–12311, October 2023.
- Z. Ying, G. Li, Y. Ren, R. Wang, and W. Wang. A new low-light image enhancement algorithm using camera response model. In *Proceedings of the IEEE International Conference on Computer Vision Workshops*, pages 3015–3022, 2017.
- L. Yuan and J. Sun. Automatic exposure correction of consumer photographs. In *European Conference on Computer Vision*, pages 771–785. Springer, 2012.
- Y. Yuan, W. Yang, W. Ren, J. Liu, W. J. Scheirer, and Z. Wang. Ug²⁺ track 2: A collective benchmark effort for evaluating and advancing image understanding in poor visibility environments. *arXiv preprint arXiv:1904.04474*, 2019.
- F. Zhang, Y. Li, S. You, and Y. Fu. Learning temporal consistency for low light video enhancement from single images. In *Proceedings of the IEEE/CVF Conference on Computer Vision and Pattern Recognition*, pages 4967–4976, 2021.
- L. Zhang, L. Zhang, X. Liu, Y. Shen, S. Zhang, and S. Zhao. Zero-shot restoration of back-lit images using deep internal learning. In *Proceedings of the 27th ACM International Conference on Multimedia*, pages 1623–1631, 2019a.
- R. Zhang, P. Isola, A. A. Efros, E. Shechtman, and O. Wang. The unreasonable effectiveness of deep features as a perceptual metric. In *Proceedings of the IEEE conference on computer vision and pattern recognition*, pages 586–595, 2018.
- Y. Zhang, J. Zhang, and X. Guo. Kindling the darkness: A practical low-light image enhancer. In *Proceedings of the 27th ACM international conference on multimedia*, pages 1632–1640, 2019b.
- Z. Zhang, H. Zheng, R. Hong, M. Xu, S. Yan, and M. Wang. Deep color consistent network for low-light image enhancement. In *Proceedings of the IEEE/CVF Conference on Computer Vision and Pattern Recognition*, pages 1899–1908, 2022.
- Z. Zhao, B. Xiong, L. Wang, Q. Ou, L. Yu, and F. Kuang. Retinexpdip: A unified deep framework for low-light image enhancement. *IEEE Transactions on Circuits and Systems for Video Technology*, 32(3): 1076–1088, 2021.
- A. Zhu, L. Zhang, Y. Shen, Y. Ma, S. Zhao, and Y. Zhou. Zero-shot restoration of underexposed images via robust retinex decomposition. In *2020 IEEE International Conference on Multimedia and Expo (ICME)*, pages 1–6. IEEE, 2020a.
- M. Zhu, P. Pan, W. Chen, and Y. Yang. Eemefn: Low-light image enhancement via edge-enhanced multi-exposure fusion network. In *Proceedings of the AAAI Conference on Artificial Intelligence*, volume 34, pages 13106–13113, 2020b.

Appendix

Notation

We first briefly summarise the notations in the paper.

- \mathbf{I} : Image
 \mathbf{L} : Illuminance
 \mathbf{R} : Reflectance
 $(\cdot)_l$: Component for the low light image
 $(\cdot)_h$: Component for the normally exposed image
 ϵ : Noise term
 δ : Quantization error
 $\Delta\mathbf{I}$: Offset term of the dynamic range compression
 \odot : Element-wise division
 \otimes : Element-wise multiplication
 α : The ratio term we want to derive in Eq. 10
 β : The offset term we want to derive in Eq. 10
 α' : The ratio term in reverse degradation process Eq. 18
 β' : The offset term in reverse degradation process Eq. 18
 k : The maximum value of intensity
 q : The least significant bit
 g : The mapping function we use

6.1 Derivation of Eq. 10

We have the expressions of DI-Retinex theory for both low light and normally exposed images as follows:

$$\begin{cases} \mathbf{I}_l = \mathcal{G}(\mathbf{L}_l \odot \mathbf{R} + \epsilon_l) + \delta_l + \Delta\mathbf{I}_l \\ \mathbf{I}_h = \mathcal{G}(\mathbf{L}_h \odot \mathbf{R} + \epsilon_h) + \delta_h + \Delta\mathbf{I}_h. \end{cases}$$

Plug the expression of \mathcal{G} .

$$\begin{cases} \mathbf{I}_l = \mu + \lambda(\mathbf{L}_l \odot \mathbf{R} + \epsilon_l)^\gamma + \delta_l + \Delta\mathbf{I}_l \\ \mathbf{I}_h = \mu + \lambda(\mathbf{L}_h \odot \mathbf{R} + \epsilon_h)^\gamma + \delta_h + \Delta\mathbf{I}_h. \end{cases}$$

By transforming the first expression, we have

$$\mathbf{R} = \left\{ \left[\frac{1}{\lambda} (\mathbf{I}_l - \delta_l - \Delta\mathbf{I}_l - \mu) \right]^{\frac{1}{\gamma}} - \epsilon_l \right\} \odot \mathbf{L}_l.$$

Plug it into the expression of extended Retinex theory for normally exposed image. Suppose $\mathbf{r} = \mathbf{L}_h \odot \mathbf{L}_l \geq \mathbf{1}$. Then we have

$$\begin{aligned} \mathbf{I}_h = & \lambda \left(\mathbf{r} \odot \left[\frac{1}{\lambda} (\mathbf{I}_l - \delta_l - \Delta\mathbf{I}_l - \mu) \right]^{\frac{1}{\gamma}} - \mathbf{r} \odot \epsilon_l + \epsilon_h \right)^\gamma \\ & + \mu + \delta_h + \Delta\mathbf{I}_h. \end{aligned}$$

According to the approximation that

$$(1+x)^n = 1+nx, \quad (25)$$

when $x \rightarrow 0$ by Taylor expansion, we can get

$$\begin{aligned} \mathbf{I}_h &\approx \lambda \mathbf{r}^\gamma \odot \left[\frac{1}{\lambda} (\mathbf{I}_l - \boldsymbol{\delta}_l - \Delta \mathbf{I}_l - \mu) \right] \\ &\quad + \lambda \gamma \mathbf{r}^{\gamma-1} (\boldsymbol{\epsilon}_h - \mathbf{r} \odot \boldsymbol{\epsilon}_l) \left[\frac{1}{\lambda} (\mathbf{I}_l - \boldsymbol{\delta}_l - \Delta \mathbf{I}_l - \mu) \right]^{\frac{\gamma-1}{\gamma}} \\ &\quad + \mu + \boldsymbol{\delta}_h + \Delta \mathbf{I}_h. \end{aligned}$$

Let the second term be

$$T = \lambda \gamma \mathbf{r}^{\gamma-1} (\boldsymbol{\epsilon}_h - \mathbf{r} \odot \boldsymbol{\epsilon}_l) \left[\frac{1}{\lambda} (\mathbf{I}_l - \boldsymbol{\delta}_l - \Delta \mathbf{I}_l - \mu) \right]^{\frac{\gamma-1}{\gamma}},$$

and use approximation in Eq. 25, thus we have

$$\begin{aligned} T &= \lambda^{\frac{1}{\gamma}} \gamma \mathbf{r}^{\gamma-1} (\boldsymbol{\epsilon}_h - \mathbf{r} \odot \boldsymbol{\epsilon}_l) (\mathbf{I}_l - \boldsymbol{\delta}_l - \Delta \mathbf{I}_l - \mu)^{\frac{\gamma-1}{\gamma}} \\ &\approx \lambda^{\frac{1}{\gamma}} \gamma \mathbf{r}^{\gamma-1} (\boldsymbol{\epsilon}_h - \mathbf{r} \odot \boldsymbol{\epsilon}_l) \\ &\quad \left[\mathbf{I}_l^{\frac{\gamma-1}{\gamma}} + \frac{1-\gamma}{\gamma} (\boldsymbol{\delta}_l + \Delta \mathbf{I}_l + \mu) \mathbf{I}_l^{\frac{-1}{\gamma}} \right]. \end{aligned}$$

Note that $\gamma \approx 0.5$, $\mathbf{r} \geq \mathbf{1}$ and thus $\mathbf{r}^{\gamma-1} \leq \mathbf{1}$. The noise term $(\boldsymbol{\epsilon}_h - \mathbf{r} \odot \boldsymbol{\epsilon}_l)$ is small. When $\mathbf{I}_l \in [1, 255]$, we have $\mathbf{I}_l^{\frac{\gamma-1}{\gamma}} \leq \mathbf{1}$ and $\mathbf{I}_l^{\frac{-1}{\gamma}} \leq \mathbf{1}$, which ensures $T \rightarrow 0$ compared to the maximum intensity of 255 for \mathbf{I}_h . When $\mathbf{I}_{l,i,j} = 0$ at (i, j) -th pixel, $\mathbf{L}_{l,i,j}$ also equals zero and thus $\mathbf{r}_{i,j} = +\infty \Rightarrow \mathbf{r}_{i,j}^{\gamma-1} \rightarrow 0$. Besides, the probability of $\mathbf{I}_{l,i,j}$ exactly equaling to zero is extremely small among pixels in reality. The second term T is thus much smaller than the other terms and can be safely omitted, which yields

$$\begin{aligned} \mathbf{I}_h &\approx \mathbf{r}^\gamma \odot (\mathbf{I}_l - \boldsymbol{\delta}_l - \Delta \mathbf{I}_l - \mu) + \mu + \boldsymbol{\delta}_h + \Delta \mathbf{I}_h \\ &= \mathbf{r}^\gamma \odot \mathbf{I}_l + [\mu + \boldsymbol{\delta}_h + \Delta \mathbf{I}_h - \mathbf{r}^\gamma \odot (\boldsymbol{\delta}_l + \Delta \mathbf{I}_l + \mu)]. \end{aligned}$$

Therefore, we can obtain

$$\mathbf{I}_h \approx \boldsymbol{\alpha} \mathbf{I}_l + \boldsymbol{\beta},$$

$$\text{where } \begin{cases} \boldsymbol{\alpha} = \mathbf{r}^\gamma = (\mathbf{L}_h \odot \mathbf{L}_l)^\gamma \\ \boldsymbol{\beta} = \mu + \boldsymbol{\delta}_h + \Delta \mathbf{I}_h - \mathbf{r}^\gamma \odot (\boldsymbol{\delta}_l + \Delta \mathbf{I}_l + \mu). \end{cases}$$

6.2 Derivation of Eq. 18

We want to show

$$\mathbf{I}_l \approx \boldsymbol{\alpha}' \mathbf{I}_h + \boldsymbol{\beta}',$$

$$\text{where } \begin{cases} \boldsymbol{\alpha}' = \mathbf{r}^{-\gamma} = (\mathbf{L}_l \odot \mathbf{L}_h)^\gamma \\ \boldsymbol{\beta}' = \mu + \boldsymbol{\delta}_l + \Delta \mathbf{I}_l - \mathbf{r}^{-\gamma} \odot (\boldsymbol{\delta}_h + \Delta \mathbf{I}_h + \mu). \end{cases}$$

Similar to the derivation of Eq. 10, we start from

$$\begin{cases} \mathbf{I}_l = \mathcal{G}(\mathbf{L}_l \odot \mathbf{R} + \boldsymbol{\epsilon}_l) + \boldsymbol{\delta}_l + \Delta \mathbf{I}_l \\ \mathbf{I}_h = \mathcal{G}(\mathbf{L}_h \odot \mathbf{R} + \boldsymbol{\epsilon}_h) + \boldsymbol{\delta}_h + \Delta \mathbf{I}_h. \end{cases}$$

and we can get

$$\begin{aligned} \mathbf{I}_l &= \lambda \left(\mathbf{r}^{-1} \odot \left[\frac{1}{\lambda} (\mathbf{I}_h - \boldsymbol{\delta}_h - \Delta \mathbf{I}_h - \mu) \right]^{\frac{1}{\gamma}} - \mathbf{r}^{-1} \odot \boldsymbol{\epsilon}_h + \boldsymbol{\epsilon}_l \right)^\gamma \\ &\quad + \mu + \boldsymbol{\delta}_l + \Delta \mathbf{I}_l. \end{aligned}$$

Then by using approximation in Eq. 25 we have

$$\begin{aligned} \mathbf{I}_l &\approx \lambda \mathbf{r}^{-\gamma} \odot \left[\frac{1}{\lambda} (\mathbf{I}_h - \boldsymbol{\delta}_h - \Delta \mathbf{I}_h - \mu) \right] \\ &\quad + \lambda \gamma \mathbf{r}^{1-\gamma} (\boldsymbol{\epsilon}_l - \mathbf{r}^{-1} \odot \boldsymbol{\epsilon}_h) \left[\frac{1}{\lambda} (\mathbf{I}_h - \boldsymbol{\delta}_h - \Delta \mathbf{I}_h - \mu) \right]^{\frac{\gamma-1}{\gamma}} \\ &\quad + \mu + \boldsymbol{\delta}_l + \Delta \mathbf{I}_l. \end{aligned}$$

Let the second term be

$$\begin{aligned} T' &= \lambda^{\frac{1}{\gamma}} \gamma \mathbf{r}^{1-\gamma} (\boldsymbol{\epsilon}_l - \mathbf{r}^{-1} \odot \boldsymbol{\epsilon}_h) (\mathbf{I}_h - \boldsymbol{\delta}_h - \Delta \mathbf{I}_h - \mu)^{\frac{\gamma-1}{\gamma}} \\ &\approx \lambda^{\frac{1}{\gamma}} \gamma \mathbf{r}^{1-\gamma} (\boldsymbol{\epsilon}_l - \mathbf{r}^{-1} \odot \boldsymbol{\epsilon}_h) \\ &\quad \left[\mathbf{I}_h^{\frac{\gamma-1}{\gamma}} + \frac{1-\gamma}{\gamma} (\boldsymbol{\delta}_h + \Delta \mathbf{I}_h + \mu) \mathbf{I}_h^{\frac{-1}{\gamma}} \right]. \end{aligned}$$

Note that $\mathbf{r} \geq \mathbf{1}$, and thus $\mathbf{r}^{-1} \geq \mathbf{1}$. The noise term $(\boldsymbol{\epsilon}_l - \mathbf{r}^{-1} \odot \boldsymbol{\epsilon}_h)$ is small. When $\mathbf{I}_h \in [1, 255]$, we have $\mathbf{I}_h^{\frac{\gamma-1}{\gamma}} \leq \mathbf{1}$ and $\mathbf{I}_h^{\frac{-1}{\gamma}} \leq \mathbf{1}$, which ensures $T' \rightarrow 0$ compared to the maximum intensity. When $\mathbf{I}_{h,i,j} = 0$ at (i, j) -th pixel, $\mathbf{L}_{h,i,j}$ also equals zero and thus $\mathbf{r}_{i,j}^{1-\gamma} \rightarrow 0$. Besides, the probability of $\mathbf{I}_{h,i,j}$ exactly equaling to zero is extremely small among pixels in reality. The second term T' is thus much smaller than the other terms and can be safely omitted, which yields

$$\begin{aligned} \mathbf{I}_l &\approx \mathbf{r}^{-\gamma} \odot (\mathbf{I}_h - \boldsymbol{\delta}_h - \Delta \mathbf{I}_h - \mu) + \mu + \boldsymbol{\delta}_l + \Delta \mathbf{I}_l \\ &= \mathbf{r}^{-\gamma} \odot \mathbf{I}_h + [\mu + \boldsymbol{\delta}_l + \Delta \mathbf{I}_l - \mathbf{r}^{-\gamma} \odot (\boldsymbol{\delta}_h + \Delta \mathbf{I}_h + \mu)]. \end{aligned}$$

Therefore, we can obtain

$$\mathbf{I}_l \approx \boldsymbol{\alpha}' \mathbf{I}_h + \boldsymbol{\beta}.$$

$$\text{where } \begin{cases} \boldsymbol{\alpha}' = \mathbf{r}^{-\gamma} = (\mathbf{L}_l \odot \mathbf{L}_h)^\gamma \\ \boldsymbol{\beta}' = \mu + \boldsymbol{\delta}_l + \Delta \mathbf{I}_l - \mathbf{r}^{-\gamma} \odot (\boldsymbol{\delta}_h + \Delta \mathbf{I}_h + \mu). \end{cases}$$

6.3 Discussion of Linear Model and the Offset $\boldsymbol{\beta}$

The expression of $\boldsymbol{\beta}$ is given by

$$\boldsymbol{\beta} = \mu + \boldsymbol{\delta}_h + \Delta \mathbf{I}_h - \boldsymbol{\alpha} \odot (\mu + \boldsymbol{\delta}_l + \Delta \mathbf{I}_l),$$

where $\boldsymbol{\alpha} = (\mathbf{L}_h \odot \mathbf{L}_l)^\gamma \geq \mathbf{1}$. We analyse the magnitude of $\boldsymbol{\beta}$ by computing its mean and variance. Given $\mathbb{E}[\boldsymbol{\alpha}] = \bar{\boldsymbol{\alpha}} > \mathbf{1}$ and $\mathbb{E}[\boldsymbol{\delta}_l] = \mathbb{E}[\boldsymbol{\delta}_h] = \mathbf{0}$ and suppose $\boldsymbol{\alpha}$ is independent of $\Delta \mathbf{I}_h$ and $\Delta \mathbf{I}_l$, we have

$$\mathbb{E}[\boldsymbol{\beta}] = \mu(1 - \bar{\boldsymbol{\alpha}}) + \mathbb{E}[\Delta \mathbf{I}_h] - \bar{\boldsymbol{\alpha}} \mathbb{E}[\Delta \mathbf{I}_l].$$

A properly exposed has equal probability of overexposure and underexposure. Thus $\mathbb{E}[\Delta\mathbf{I}_h] = 0$. Also a negative overflow exceeding 0 caused by a negative image irradiance is seldom and thus $\mathbb{E}[\Delta\mathbf{I}_l] \rightarrow 0$. μ is a negative number such that the Gamma transformation can map $[0, +\infty)$ to $[0, 255]$. $(1 - \bar{\alpha}) < -1$ (found in the following statistical experiments) makes the magnitude of $\mathbb{E}[\beta]$ significant. Even if $\mu(1 - \bar{\alpha}) = \bar{\alpha}\mathbb{E}[\Delta\mathbf{I}_l]$ in some rare case, $\Delta\mathbf{I}_l$ has non-zero values only in some regions of an image and $\mu(1 - \bar{\alpha})$ has large values in the regions where $\Delta\mathbf{I}_l$ has zero values. Therefore, β is not negligible in terms of considerable mean.

We then compute β 's variance. The variance of μ is zero as it is a constant. Since the quantization error follows a uniform distribution from $q/2$ to $q/2$, its variance is $q^2/12$. Note that with the assumption of flux consistency along time dimension across spatial pixels during receiving radiance in a short period, α can be further treated as a constant matrix. So it can be considered as a scalar α when computing β 's variance,

$$\begin{aligned} \text{Var}(\beta) &= (q^2/12) + \text{Var}(\Delta\mathbf{I}_h) + \alpha^2 ((q^2/12) + \text{Var}(\Delta\mathbf{I}_l)) \\ &= (1 + \alpha^2)(q^2/12) + \text{Var}(\Delta\mathbf{I}_h) + \alpha^2 \text{Var}(\Delta\mathbf{I}_l). \end{aligned}$$

As shown, the factor of α^2 enlarges the variance of β . The amplified variance also makes β non-negligible.

6.4 Discussion on Reverse Degradation

The expression of β' is given by

$$\beta' = \mu + \delta_l + \Delta\mathbf{I}_l - \alpha' \odot (\mu + \delta_h + \Delta\mathbf{I}_h),$$

where $\alpha' = (\mathbf{L}_l \otimes \mathbf{L}_h)^\gamma \leq 1$. We analyse the magnitude of β' by computing its mean and variance. Given $\mathbb{E}[\alpha'] = \bar{\alpha}' \in [0, 1]$ and $\mathbb{E}[\delta_h] = \mathbb{E}[\delta_l] = 0$ and suppose α' is independent of $\Delta\mathbf{I}_h$ and $\Delta\mathbf{I}_l$, we have

$$\mathbb{E}[\beta'] = \mu(1 - \bar{\alpha}') + \mathbb{E}[\Delta\mathbf{I}_l] - \bar{\alpha}'\mathbb{E}[\Delta\mathbf{I}_h].$$

A properly exposed has equal probability of overexposure and underexposure. Thus $\mathbb{E}[\Delta\mathbf{I}_h] = 0$. Also a negative overflow exceeding 0 caused by a negative image irradiance is seldom and thus $\mathbb{E}[\Delta\mathbf{I}_l] \rightarrow 0$. μ is a negative number such that the Gamma transformation can map $[0, +\infty)$ to $[0, 255]$. $1 - \bar{\alpha}' \in [0, 1]$. This makes $\mathbb{E}[\beta'] \approx \mu(1 - \bar{\alpha}')$ getting small. For even more safely removing β' , we compute reverse degradation loss in Gamma space by taking a power of $\frac{1}{\gamma}$, which suppresses the magnitude of β' .

We then compute the variance of β' . Similar to Section 6.3, we can get

$$\begin{aligned} \text{Var}(\beta) &= (q^2/12) + \text{Var}(\Delta\mathbf{I}_l) + \alpha'^2 ((q^2/12) + \text{Var}(\Delta\mathbf{I}_h)) \\ &= (1 + \alpha'^2)(q^2/12) + \text{Var}(\Delta\mathbf{I}_l) + \alpha'^2 \text{Var}(\Delta\mathbf{I}_h), \end{aligned}$$

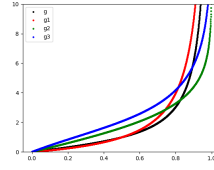


Fig. 18: The curves of four used mapping functions.

where α' represents the scalar form of α , assuming flux consistency across spatial pixels over a brief time period when receiving radiance. As depicted, the factor α'^2 assumes a small value, given that α' is less than 1 while the max pixel value is 255. The variance of β' closely approximates $(q^2/12) + \text{Var}(\Delta\mathbf{I}_l)$, which denotes the variance arising from error and offset terms in low-light images. It is important to note that the variance is small and thus approaching zero.

6.5 Discussion on Mapping Function g and Contrast Brightness Algorithm

We use four nonlinear function mapping $[-1, 1]$ to $[0, +\infty)$. According to the finding of statistical experiments in Section 6.3. The ratio between the exposures of low light and normally exposed images is mainly within $[1, 10]$, we thus make sure that most output values of mapping function lie in the region. The formula of four used functions are given below and their curves are drawn in Fig. 18.

$$\begin{aligned} g(c) &= \tan\left(\frac{45 + (45 - \tau)c}{180}\pi\right) \\ g_1(c) &= \frac{1 + c}{1 - c + e} \\ g_2(c) &= 3 \tanh^{-1}\left(\frac{1}{2} + \frac{1}{2}c\right) = \frac{3}{2} \log\left(\frac{3 + c}{1 - c + e}\right) \\ g_3(c) &= 3 \log(g(c) + 1). \end{aligned}$$

A shifted reciprocal function like g_1 is a straightforward and common choice. But we can see that g_1 has an extremely steep rise when $c > 0.8$ and thus generates the worst result in Table. 4. To alleviate the steep rise, we apply a logarithm function to shifted g_1 and form g_2 . It coincidentally becomes a shifted inverse hyperbolic tangent function. But it still cannot lead to a good enough performance. Then we choose a tangent function g and its performance is satisfactory. We further try its logarithm g_3 with a gentler slope. It has even better effect but the nesting of two nonlinear functions yields more computations. Considering the trade-off, we just use g .

The majority of existing works about image contrast enhancement are based on histogram equalization (Padmavathy and Priya, 2018; Vijayalakshmi et al., 2020; Park et al., 2018). Though some variants of Eq. 17 is used empirically in industry for adjusting image's contrast, there is no academic paper

discussing it to the best of our knowledge. One of our contributions lies in employing it to solve low light enhancement problem with the zero-reference regulation of two losses. Compared with other functions with single coefficient, the formula involving two coefficients is more difficult for a neural network to learn. Our derived reverse degradation loss and variance suppression loss can effectively guide the network to learn the coefficient pair of the adjustment function. We experiment various mapping functions g aforementioned and modified the original formulation with the best choice of g .

6.6 Network Structure

Our model is extremely simple and its structure is shown in Table 6.

Table 6: The structure of the network. C_{int} and C_{out} are the internal and output channel and are specified in paper. The output is split for \mathbf{b} and \mathbf{c}

layer	channel_in	channel_out	kernel	stride	padding
Conv+ReLU	3	C_{int}	3	1	1
Conv+ReLU	C_{int}	C_{int}	3	1	1
Conv+Tanh	C_{int}	C_{out}	3	1	1

6.7 Decomposition Visualization

We showcase an visual example of decomposition of our enhancement model in Fig. 19.

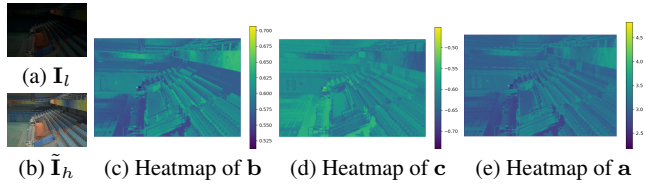


Fig. 19: The decomposition results of the model.